HHS Public Access

Author manuscript

Cell Rep. Author manuscript; available in PMC 2024 October 11.

Published in final edited form as:

Cell Rep. 2024 August 27; 43(8): 114589. doi:10.1016/j.celrep.2024.114589.

Regulation of MYC by CARD14 in human epithelium is a determinant of epidermal homeostasis and disease

Stanley B. DeVore[1,2,3], **Matthew Schuetz**[2], **Lauren Alvey**[1], **Henry Lujan**[2], **David E. Ochayon**[2], **Lindsey Williams**[2], **Wan Chi Chang**[2], **Alyssa Filuta**[2], **Brandy Ruff**[2], **Arjun Kothari**[2], **Jennifer M. Hahn**[4], **Eric Brandt**[2], **Latha Satish**[1,2], **Krishna Roskin**[5], **Andrew B. Herr**[1,6], **Jocelyn M. Biagini**[1,2], **Lisa J. Martin**[1,2,7], **Deniz Cagdas**[8], **Sevgi Keles**[9], **Joshua D. Milner**[10], **Dorothy M. Supp**[4,11], **Gurjit K. Khurana Hershey**[1,2,12,*]

[1]Department of Pediatrics, University of Cincinnati College of Medicine, Cincinnati, OH 45267, USA

[2]Division of Asthma Research, University of Cincinnati College of Medicine, Cincinnati, OH 45267, USA

[3]Division of Human Genetics, University of Cincinnati College of Medicine, Cincinnati, OH 45267, USA

[4]Department of Surgery, University of Cincinnati College of Medicine, Cincinnati, OH 45267, USA

[5]Division of Biomedical Informatics, University of Cincinnati College of Medicine, Cincinnati, OH 45267, USA

[6]Division of Immunobiology, University of Cincinnati College of Medicine, Cincinnati, OH 45267, USA

[7]Division of Biostatistics, Cincinnati Children's Hospital Medical Center, Cincinnati, OH 45229, USA

[8]Division of Pediatric Immunology, Department of Pediatrics, Hacettepe University Medical School, Ihsan Dogramaci Children's Hospital, Institutes of Child Health, Ankara 06230, Turkey

[9]Division of Pediatric Immunology and Allergy, Necmettin Erbakan University, Konya 42090, Turkey

[10]Department of Pediatrics, Columbia University, New York, NY 10027, USA

[11]Scientific Staff, Shriners Children's Ohio, Dayton, OH 45404, USA

[12]Lead contact

[*]Correspondence: gurjit.hershey@cchmc.org.

AUTHOR CONTRIBUTIONS

Study design: S.B.D. and G.K.K.H. Data acquisition: S.B.D., M.S., L.A., H.L., D.E.O., L.W., A.F., B.R., J.M.H., E.B., L.S., J.M.B., D.C., S.K., J.D.M., and D.M.S. Data analysis: S.B.D., H.L., W.C.C., A.K., K.R., A.B.H., and L.J.M. Provision of reagents: J.M.H. and D.M.S. Manuscript authorship: S.B.D. and G.K.K.H.

SUPPLEMENTAL INFORMATION

Supplemental information can be found online at https://doi.org/10.1016/j.celrep.2024.114589.

DECLARATION OF INTERESTS

Aspects of this manuscript have been included in a recent patent filing.

SUMMARY

Caspase recruitment domain family member 14 (CARD14) and its variants are associated with both atopic dermatitis (AD) and psoriasis, but their mechanistic impact on skin barrier homeostasis is largely unknown. CARD14 is known to signal via NF-κB; however, CARD14-NF-κB signaling does not fully explain the heterogeneity of CARD14-driven disease. Here, we describe a direct interaction between CARD14 and MYC and show that CARD14 signals through MYC in keratinocytes to coordinate skin barrier homeostasis. CARD14 directly binds MYC and influences barrier formation in an MYC-dependent fashion, and this mechanism is undermined by disease-associated CARD14 variants. These studies establish a paradigm that CARD14 activation regulates skin barrier function by two distinct mechanisms, including activating NF-κB to bolster the antimicrobial (chemical) barrier and stimulating MYC to bolster the physical barrier. Finally, we show that CARD14-dependent MYC signaling occurs in other epithelia, expanding the impact of our findings beyond the skin.

Graphical abstract

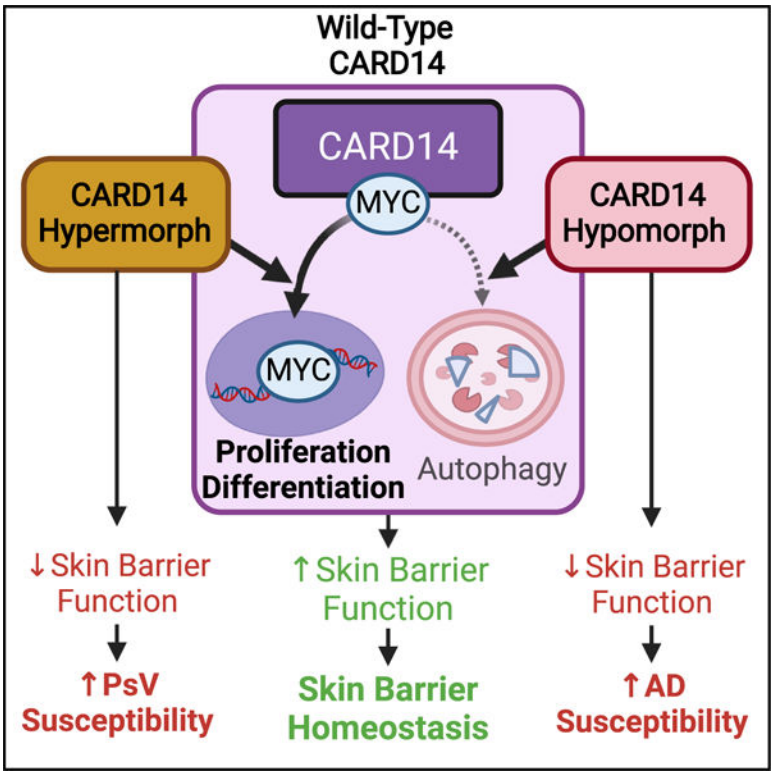

In brief

The epithelial protein CARD14 canonically regulates NF-κB and is associated with atopic dermatitis and psoriasis. DeVore et al. report that CARD14 also regulates MYC signaling to influence barrier homeostasis—a mechanism altered by disease-associated genetic variants. This pathway may represent a potential therapeutic target in diseases of dysregulated barrier function.

INTRODUCTION

Atopic dermatitis (AD) impacts nearly 20% of children worldwide and portends the development of other allergic diseases via the atopic march.[1] Skin barrier dysfunction is a key pathogenic contributor to AD; the transcutaneous passage of allergens through a leaky epidermal barrier promotes the sensitization and local inflammation that primes local and distal allergic disease.[1] Barrier dysfunction also underlies other epithelial diseases (e.g., psoriasis, food allergy) and even systemic autoimmune diseases,[2] and the extent of dysfunction correlates with disease severity.[2,3] Understanding the mechanisms underlying epithelial barrier homeostasis and dysfunction is thus crucial for developing novel strategies for the prevention and treatment of not only a spectrum of human skin diseases but also a wide range of pathologies in other epithelia.

Barrier homeostasis relies on a coordinated balance between the proliferation and differentiation of epithelial cells. Within the skin, proliferating basal keratinocytes repopulate the epidermis, while suprabasal differentiation gives rise to the structural components required for an optimally protective barrier. On such protein is filaggrin (FLG)[4]; reduced FLG is associated with barrier dysfunction and is a significant risk factor for AD and atopy.[5,6] Our group recently identified the signaling protein caspase recruitment domain family member 14 (CARD14) and its common missense variant rs11652075 (C>T, p.R820W, minor allele frequency [MAF] = 0.477) as *FLG* regulators in a genome-wide association study (GWAS) of the Mechanisms of Progression of Atopic Dermatitis to Asthma in Children (MPAACH) cohort, the first US-based cohort of children with AD.[7] CARD14 is expressed in epithelial and mucosal tissues.[8] Canonically, activated CARD14 recruits B cell lymphoma/leukemia 10 and mucosa-associated lymphoid tissue lymphoma translocation protein 1 (MALT1) to form a “CBM complex” that induces nuclear factor κB (NF-κB) and MAPK signaling.[9] Importantly, *CARD14* and its genetic variants, although rare, are implicated in the pathogenesis of AD, psoriasis, and other inflammatory skin diseases.[10,11] Despite these strong associations, the breadth of the impact of *CARD14* and its variants on epithelial homeostasis, as well as the underlying mechanisms, are not fully understood.

Here, we demonstrate an MYC regulatory pathway whereby CARD14 is a direct regulator of MYC, and that disease-associated CARD14 variants perturb this mechanism in keratinocytes to promote skin barrier dysfunction. Consistent with the known roles of MYC in the skin,[12] we further demonstrate that the CBM and CARD14 variants influence keratinocyte proliferation, epidermal differentiation, and skin barrier function. Finally, we provide evidence that the CARD14-MYC pathway may contribute to barrier homeostasis and disease pathogenesis in other *CARD14*-expressing epithelia (i.e., esophageal, nasal and airway epithelia), thus extending the impact of our findings beyond the epidermis.

RESULTS

The AD-associated R820W variant, like other disease-associated CARD14 variants, affects NF-κB signaling Using the expanded MPAACH cohort with known *CARD14* rs11652075 genotypes, we confirmed our previous finding[7] that the T allele (TT), which encodes

the CARD14 R820W substitution, is associated with reduced *FLG* in non-lesional (NL) skin (Figure 1A; Table S1). However, the mechanisms underlying this association are largely unknown. Despite its frequency, strong evolutionary conservation of basic amino acid residues at the 820 position and multiple algorithms suggest intolerance to the R820W substitution (Figure S1A; Table S2).[13–16] Two other *CARD14* mutations (I593T and N737H) have been associated with AD and have hypomorphic effects on NF-κB signaling[11]; thus, we hypothesized that R820W behaves similarly. To test this, we examined the mRNA expression level of the antimicrobial peptide (AMP) gene *S100A8*,[17] a known CARD14-NF-κB target gene, in the NL skin of individuals homozygous for the TT genotype vs. the CC or CT genotypes, and found reduced mRNA expression levels in TT individuals (Figure 1B). Further supporting the hypothesis that R820W has a hypomorphic effect on NF-κB signaling, NF-κB luciferase reporter assays showed reduced NF-κB activation by CARD14 constructs expressing the R820W protein compared to WT protein (Figure 1C). As expected, CARD14 constructs expressing R820W elicited less NF-κB activity than those expressing the psoriasis-associated[10] gain-of-function (GoF) mutation E138A. Notably, R820W protein elicited more NF-κB activity than CARD14 harboring either of the AD-associated hypomorphic N737H and I593T mutations. These data show that within a spectrum of functional CARD14 variants, the R820W variant has a hypomorphic effect on NF-κB signaling with respect to WT.

The *CARD14* R820W variant and MALT1 inhibition reduce MYC transcriptional signatures

Although altered CARD14-NF-κB signaling is known to contribute to several epidermal diseases, it is notable that there are several described psoriasis-associated *CARD14* variants (e.g., R38C, H171N) that do not hyperactivate NF-κB as would be expected.[18] This observation suggests that CARD14 variants, including R820W, may affect keratinocyte function and influence barrier homeostasis and disease by signaling through cellular pathways in addition to NF-κB.

To investigate additional pathways affected by R820W, we compared the transcriptomes of *CARD14* $^{C/C}$ (“WT”) versus isogenic CRISPR-edited *CARD14* $^{T/T}$ (“R820W”) HaCaT keratinocytes[7] either with the vehicle DMSO (“V”) or with treatment with the MALT1 inhibitor mepazine (“M”) (Figures 1D and S1B). The most significantly downregulated gene sets in vehicle-treated R820W cells vs. WT cells by gene set enrichment analysis (GSEA) were Hallmark MYC Targets V1 and Hallmark MYC Targets V2 (Figures 1E, S1C, and S1D). Ingenuity Pathway Analysis (IPA) also predicted that MYC is a crucial upstream regulatory protein inhibited in R820W + V cells, that MYC’s antagonist Max dimerization protein 1 (MAD, encoded by *MXD1*)[19] is activated in R820W cells (Figures 1F and 1G), and that R820W cells have perturbations in several MYC-associated cellular functions (Figure 1H). Further supporting the negative effect of R820W on MYC, Integrated Library of Integrated Network-Based Cellular Signatures transcriptomic analysis[20] positively correlated the R820W signature with those of cells deficient in *MYC* and cells treated with inhibitors of the MYC activator ERK[21] (Table S3). Mepazine-treated R820W and WT cells also had attenuated MYC signatures compared to their respective vehicle-treated cells and to each other (Figure S2), indicating that MALT1 signaling also contributes to MYC activity. The altered MYC signatures were also validated in RNA sequencing (RNA-seq)

results generated using a separate sequencing analysis package, EdgeR.[22] Several studies have demonstrated a crucial role for MYC signaling on keratinocyte proliferation and differentiation[12]; thus, we decided to investigate the influence of CARD14 signaling on MYC and further explore the effects of their interplay on keratinocyte and barrier function.

MYC levels are reduced but MYC autophagy is elevated in R820W and mepazine-treated keratinocytes

Supporting the sequencing, cellular MYC protein levels were reduced in R820W cells and mepazine-treated cells (Figures 2A and 2B). Levels of the MYC antagonist MAD were unchanged, but the ratio of MYC:MAD was reduced in R820W and mepazine-treated cells. The lack of statistical significance of the ANOVA interaction term indicates that the effects of the R820W genotype and mepazine treatment on MYC occur independently of each other. Notably, mepazine did not reduce MYC protein in *CARD14*-deficient ("KO" [knockout]) HaCaT keratinocytes[7] (Figures S3A and S3B), indicating that the suppressive effect of MALT1 on MYC levels is *CARD14* dependent. Similarly, nuclear localization of MYC was additively reduced in R820W and mepazine-treated cells, and the effect of MALT1 was eliminated in KO cells (Figures 2C, 2D, and S3C–S3F). These data show that CARD14 signaling affects the amount of cellular MYC protein as well as its nuclear localization, thereby supporting the existence of a CARD14-MYC pathway in keratinocytes.

We next sought to determine how CARD14 signaling impacts MYC mechanistically. MALT1 upregulates *MYC* expression in regulatory T cells downstream of CARD11,[23] so we first looked for an effect of CARD14 on *MYC* transcription. Despite observing altered *MYC* counts in our sequencing data, the levels and stability of both *MYC* and *MXD1* (encoding MAD) were unchanged by qPCR (Figures S3G and S3L). However, the half-life of MYC (but not MAD) protein was shorter in both R820W and mepazine-treated cells (Figures S4A–S4C), suggesting differential degradation of MYC protein. Proteasome inhibition did not rescue MYC levels, and ERK signaling (which attenuates the proteasomal degradation of MYC[21]) was not reduced in R820W or mepazine-treated cells, indicating MYC degradation is proteasome independent (Figures S4D–S4G).

In contrast, the autophagy inhibitor bafilomycin caused an increase in MYC protein accumulation in R820W and mepazine-treated cells, indicating increased MYC autophagic flux in these conditions (Figures 2E and 2G). Although the effect of mepazine was independent of CARD14 genotype, mepazine did not increase MYC autophagic flux in *CARD14*-deficient KO cells, indicating that MALT1-mediated MYC autophagy is CARD14 dependent (Figures S4H and S4I). However, nonselective (bulk) autophagy, as measured by autophagic flux of the autophagic mediator LC3B, was decreased in R820W and mepazine cells (in agreement with prior studies[24]) and was CARD14 independent (Figures 2F, 2G, S4J, and S4K). These data together indicate that the primary mediator of MYC degradation in R820W- and MALT1-inhibited cells is selective (rather than nonselective) autophagy and that this mechanism is dependent on CARD14.

CARD14 and MYC directly bind in keratinocytes and are dependent on CARD14 activation status and the presence of disease-associated CARD14 variants

Given the dependence of MYC degradation on CARD14, we next investigated whether the CARD14 protein directly associates with MYC. Indeed, MYC immunoprecipitated with CARD14 (Figure 3A). MYC did not immunoprecipitate with CARD10, which is also expressed in keratinocytes[25] (Figure S5A). Proximity ligation assays (PLAs) subsequently demonstrated that CARD14 and MYC co-localize within ~40 nm[26] in both co-transfected HaCaT cells and engineered skin substitutes[27] that we generated from patient-matched primary keratinocytes and fibroblasts of each homozygous genotype (Figures 3B, 3C, S5B, and S5C; primary cell characteristics in Table S4). These data strongly suggest a direct interaction between the CARD14 and MYC proteins. *In silico* modeling identified a strong candidate binding interaction between MYC and CARD14 (Figure 3D). We next co-expressed CARD14 and MYC in the presence of the small molecule 10058-F4, an MYC-MAX dimerization inhibitor that binds MYC within its predicted CARD14 binding site. Notably, prolonged (i.e., 24 h) treatment with 10058-F4 reduced CARD14-MYC binding (Figure 3E), thereby supporting the interaction predicted by our modeling data.

To examine the effects of CARD14 variants and signaling on CARD14-MYC binding, we transfected KO HaCaT cells with different CARD14 variant constructs and stimulated CARD14 signaling with phorbol myristate acetate (PMA) and ionomycin. Notably, CARD14 stimulation noticeably reduced MYC binding to $CARD14^{WT}$ but not $CARD14^{R820W}$ (Figure S5D), thereby suggesting that CARD14-MYC binding is altered by both CARD14 activation and mutation status. Consistent with this, keratinocytes expressing GoF $CARD14^{E138A}$ had significantly fewer FLAG-MYC PLA puncta per cell (indicating fewer instances of CARD14-MYC interaction) than $CARD14^{WT}$. Alternatively, cells expressing $CARD14^{R820W}$ and the AD-associated $CARD14^{I593T}$ hypomorphic variant had significantly more PLA puncta than WT, indicating maintained points of CARD14-MYC interaction with these variants. Although puncta numbers per cell trended higher in cells expressing the AD-associated $CARD14^{N737H}$ hypomorph, this was not significant (Figures 3F and 3G). Together, these data support that CARD14 not only directly binds MYC but also that this interaction is modulated by both CARD14 activation and genetic variants associated with both AD and psoriatic diseases.

CARD14-MYC signaling regulates keratinocyte proliferation and epidermal barrier function

Given this CARD14-MYC interaction and the altered MYC signatures we observed in R820W versus WT cells, we hypothesized that CARD14 influences MYC-associated keratinocyte functions. To assess this, we first utilized WT and R820W HaCaT keratinocytes whose isogenic properties allowed more accurate functional comparisons than primary keratinocytes that exhibit considerable heterogeneity. We noted reduced cellular proliferation in R820W HaCaT keratinocytes compared to WT, and although mepazine also attenuated proliferation, this was not completely CARD14 dependent (Figures 4A, 4B, and S6A–S6C). MYC, as well as the CARD14 paralogs CARD9 and CARD11, are known to influence mitochondrial function[23,28]; however, we did not detect differences in mitochondrial mass, membrane potential, nor ATP production in R820W versus WT keratinocytes (Figures S6D–

S6G). We also did not detect an effect of R820W or mepazine on keratinocyte migration as measured by wound healing "scratch" assays (Figure S6H).

MYC is known to promote suprabasal epidermal differentiation.[12] HaCaT keratinocytes do not reliably form a functional barrier, limiting our ability to test this particular MYC-associated phenotype with isogenic cell lines. Thus, despite their genetic variability, we instead differentiated *CARD14* $^{C/C}$ and *CARD14* $^{T/T}$ primary keratinocyte strains (Table S4) at the air-liquid interface (ALI) and monitored longitudinal barrier function by measuring transepithelial electrical resistance (TEER; Figure 4C). *CARD14*$^{T/T}$ primary keratinocytes had a lower maximum TEER than *CARD14* $^{C/C}$ primary keratinocyte strains (Figure 4D), showing that the R820W variant negatively impacts barrier function. Furthermore, incubation with mepazine and/or the MYC inhibitor 10058-F4 reduced maximum barrier function and fold change in TEER from days 6–8 (when TEER curves were steepest; Figures 4E–4G), indicating that optimal barrier function is also dependent on MALT1 and MYC signaling. Although the full thickness of the ALIs were similar, MYC inhibition decreased stratum corneum (SC) thickness, and in mepazine-treated ALIs, the SC represented a reduced proportion of the full thickness (Figures 4H, 4I, and S7A), suggesting interrupted epidermal differentiation. As observed in HaCaT keratinocytes, MYC expression in primary keratinocytes was lower in the context of *CARD14* $^{T/T}$ strains or with mepazine (Figures 4J and 4K). Although levels of the MYC antagonist MAD were unchanged, the ratio of MYC:MAD protein also trended lower (Figures S7B–S7D). As in HaCaTs, *MYC* and *MXD1* mRNA levels were predominantly unchanged (Figures S7E and S7F). In alignment with the MPAACH GWAS,[7] total FLG protein was lower in *CARD14* $^{T/T}$ ALIs (Figures 4L, 4M, and S7G). MALT1 and MYC inhibition additively suppressed FLG protein in *CARD14* $^{C/C}$ ALIs but not *CARD14* $^{T/T}$ ALIs, likely due to lower baseline expression and high variability. MYC inhibition suppressed *FLG* mRNA, but we were underpowered to detect baseline changes by genotype or treatment (Figure S7H). Together, these data highlight that the hypomorphic R820W variant, MYC antagonism, and MALT1 inhibition attenuate keratinocyte proliferation, differentiation, and barrier function, thereby supporting a crucial role for CARD14-MYC signaling in processes necessary for epidermal homeostasis and protection from AD.

CARD14-MYC signaling promotes keratinocyte differentiation *in vivo*

To build on our observations that CARD14-MYC signaling contributes to epidermal differentiation and homeostasis, we next used pre-existing single-cell RNA-seq (scRNA-seq) data from healthy neonatal foreskin.[29] Using established marker genes, we combined keratinocyte Louvain clusters into three cell populations, each reflecting a major epidermal layer: basal, spinous, and granular (Figures S8A–S8D). The granular population encompasses cells from both the granular and corneal layers due to the small number of corneocytes sequenced. Within all three populations, MYC^+/$CARD14^+$ cells had significantly upregulated MYC signatures compared to MYC^+/$CARD14^-$ cells despite similar MYC expression levels (Figures 5A–5C and S8E). Given the differentiation-promoting effects of MYC in the skin,[12] we hypothesized that the transcriptomes of cells with detectable CARD14 expression would reflect a more advanced differentiation state than those with undetectable CARD14 expression. Indeed, compared to MYC^+/$CARD14^-$ cells,

the differentially expressed genes in MYC^{+}/CARD14^{+} cells were significantly enriched for Gene Ontology (GO) terms related to epidermal or skin differentiation and keratinization, particularly within the more superficial spinous and granular populations (Figure 5D). In contrast, the same GO terms were largely unchanged between MYC^{-}/CARD14^{+} and MYC^{-}/CARD14^{-} cells, indicating that the pro-differentiation effect of CARD14 is MYC dependent (Figure S8F). These data strongly support a role for CARD14-MYC interactions in keratinocyte differentiation and epidermal homeostasis *in vivo*.

MYC signaling is altered downstream of pathogenic CARD14 variants

The impact of *CARD14* missense variants on inflammatory skin diseases is often attributed solely to altered NF-κB signaling, with GoF variants causing psoriatic disease and loss-of-function (LoF) variants causing AD.[10] However, our data have shown that concomitant perturbation of MYC signaling likely contributes to these CARD14-driven diseases as well (Figure 5E). Indeed, compared to healthy skin, psoriasis vulgaris (PsV) and generalized pustular psoriasis (GPP) skin harboring the CARD14 GoF mutations G117S and E138A GoF exhibited elevated MYC signatures (Figures 5F and 5G).[30] Paralleling their relative NF-κB-activating capacities, MYC signatures in E138A skin were higher than those in G117S skin (Figure S9A).[18] Likewise, skin MYC signatures were strongly and persistently upregulated after inducing expression of the GoF *Card14*^{E138A} gene in mice (Figures 5H, S9B, and S9C).[31] Notably, other studies have shown that both humans and mice harboring E138A or similar GoF mutations have greater epidermal thickness and expression of terminal differentiation markers, including the crucial barrier gene *FLG*.[17,31–34]

To further examine the effect of hypomorphic CARD14 variants on MYC, we performed RNA-seq analysis on KO HaCaTs transfected with plasmids expressing CARD14^{WT} or CARD14 harboring each of the AD-associated hypomorphic variants (R820W, I593T, and N737H; Figure 5I). Confirming our sequencing in isogenic WT and R820W HaCaTs, cells expressing CARD14^{R820W} had reduced MYC signatures compared to those expressing CARD14^{WT} (Figure 5J). Similarly, MYC signatures were decreased in cells expressing CARD14^{I593T} (Figure 5K).

Interestingly, MYC signatures were unchanged in cells expressing CARD14^{N737H} despite its known suppressive effect on NF-κB (Figure 5L).[11] These data indicate that N737H primarily exerts its pro-AD effect by suppressing NF-κB, in contrast to the I593T and R820W variants, which suppress both MYC and NF-κB. This finding uncouples CARD14-MYC from CARD14-NF-κB signaling, indicating that these two CARD14-dependent signaling pathways may independently contribute to the pathogenesis of inflammatory skin diseases. Importantly, in agreement with this, we found that the psoriasis-associated *CARD14* mutations (e.g., R38C, H171N) that do not hyperactivate NF-κB[18] (which prompted our initial RNA-seq experiment) instead upregulate MYC signatures compared to WT CARD14 and even NF-κB-inducing GoF mutations (Figures S9D and S9E). These data build on the existing model of CARD14-driven inflammatory disease by offering perturbed CARD14-MYC signaling as an independent or complementary mechanism to altered CARD14-NF-κB signaling.

MYC signaling is preserved in the absence of CARD14

In contrast to the suppressed MYC signatures with hypomorphic CARD14 mutations, we observed that KO HaCaT cells had an MYC signature similar to isogenic WT cells but upregulated compared to R820W cells (Figures 6A and 6B). This observation prompted us to hypothesize that, in contrast to active MYC degradation in the context of hypomorphic CARD14 variants, MYC remains intact and capable of maintaining barrier homeostasis in CARD14-deficient conditions. Supporting this, nuclear MYC in KO cells was comparable to WT but greater than R820W cells (Figures 6C and 6D), while MYC autophagic flux in KO cells was comparable to WT but less than R820W cells (Figures 6E and 6F). Furthermore, transcriptional data from previous murine studies revealed that Card14-deficient (*Card14*$^{-/-}$) mice have MYC signatures comparable to those of Card14-sufficient (*Card14*$^{+/+}$) mice (Figure 6G) and have similar expression levels of Ki67 and terminal differentiation markers.[32,35] Importantly, there were no appreciable phenotypic differences between Card14-deficient and Card14-sufficient mice that would suggest spontaneous AD development (Figure 6H). There were also no significant alterations in baseline epidermal thickness or transepidermal water loss (TEWL), a measure of barrier function (Figures 6I–6K). Nuclear MYC staining was also similar (Figure 6L). These studies highlight that CARD14 deficiency does not result in altered epidermal structure or function, in part due to retained homeostatic MYC signaling.

AD is absent in a rare case of human CARD14 deficiency

Consistent with our *in vitro* and mouse data, we recently identified a patient with CARD14 deficiency without any overt skin barrier defect. The 3.5-month-old infant, born at term to consanguineous parents, presented with fever, cough, and moniliasis at 15 days old and was hospitalized for pneumonia. No skin involvement was noted. His family history was significant for a cousin with severe combined immunodeficiency (SCID) due to a homozygous Artemis deficiency (c.110A>G). The patient was found to have lymphopenia (623/mm^3), mild neutropenia (1,110/mm^3), and low serum immunoglobulin levels (immunoglobulin G [IgG] 487 mg/dL [receiving intravenous Ig therapy], IgM <4.17 mg/dL, IgA <6.67 mg/dL, IgE 18.5 IU/mL). Lymphocyte subset analyses revealed T cell-negative, B cell-negative, NK cell-positive SCID with oligoclonal proliferation. Exome sequencing confirmed Artemis SCID, but incidentally identified homozygous truncating *CARD14* mutations (rs772958714; c.892C>T; p.R298X) (Figure 6M). The patient subsequently received a human leukocyte antigen-matched hematopoietic stem cell transplant (HSCT) without a conditioning regimen, which fully engrafted. His HSCT had no significant sequelae other than nail dystrophy and autoimmune alopecia, which presented approximately 2.5 and 6 years later, respectively. Other than his alopecia, the patient has never exhibited any skin findings nor AD lesions to date despite his CARD14 deficiency and the propensity of patients with SCID to develop dermatitis.[36] Although several genetic databases lack additional patients with CARD14 deficiency,[37–39] the Genome Aggregation Database predicts that *CARD14* is tolerant to LoF variants (observed/expected score = 0.75 [95% confidence interval {CI} = 0.58–0.99]).[39] These data collectively support our hypothesis and our observations in cells and mice that epidermal barrier function is preserved in the context of CARD14 deficiency, perhaps due to preserved MYC signaling.

Altered CARD14-MYC signaling may contribute to barrier homeostasis and allergic disease in other epithelial tissues

We next used published transcriptomic data to further explore the role of CARD14-MYC signaling and CARD14 variants in both healthy and diseased skin, as well as in other epithelial tissues. Since rs11652075 is exonic, we used RNA-seq FASTQ files (where available) to infer the genotypes of each subject, thereby allowing us to make comparisons between them (Figure 7A). Corroborating our *in vitro* data, we detected reduced MYC signatures within the healthy skin of *CARD14* $^{T/T}$ versus *CARD14* $^{C/C}$ individuals (Figure 7B).[40] We next looked for elevated MYC signaling in psoriatic skin, where increased interleukin-17A (IL-17A) signaling through keratinocyte IL-17R is known to hyperactivate CARD14.[10,32,41] Indeed, MYC signatures were upregulated in psoriatic versus healthy skin in two separate studies.[40,42] Furthermore, and consistent with the literature,[18,41,43] patients with psoriasis were significantly enriched for the CARD14^{WT}-encoding C allele that elicits greater MYC activity than the CARD14^{R820W}-encoding TT (Figures 7C, S9F, and S9G). Furthermore, we found that treatment with anti-IL-17A biologic secukinumab attenuated MYC signatures in psoriatic skin (Figures S9H and S9I), which is consistent with a theoretical decrease in IL-17R-driven CARD14-MYC signaling.

CARD14 is also expressed in the esophageal mucosa and airway epithelia,[8] and individuals with severely hypomorphic CARD14 mutations (N737H and I593T) exhibit both food allergy and allergic asthma.[11] Because of this, we next looked for signs of altered CARD14-MYC signaling in other epithelia. MYC signatures were similar in healthy *CARD14* $^{T/T}$ versus *CARD14* $^{C/T}$ esophagi (note that no healthy *CARD14* $^{C/C}$ individuals were identified)[44]; however, signatures trended downward in esophagi affected by eosinophilic esophagitis[45] (EoE) compared to healthy esophagi (Figures 7D and 7E). Additionally, patients with EoE were enriched for the rs11652075 TT (Figure S9J), strongly suggesting a pathogenic role for *CARD14* and the R820W variant in EoE. We also detected reduced MYC signatures within the bronchi of individuals with T helper 2 cell (Th2)-high asthma (Figure 7F)[46] and in the nasal epithelia of individuals with eosinophilic chronic rhinosinusitis with nasal polyps (CRwNP) compared to healthy controls (Figure 7G).[47] Together, these data suggest that CARD14- and rs11652075-dependent MYC signaling could contribute to homeostasis, pathogenesis, and treatment responses in not only the skin but also other CARD14-expressing epithelial tissues.

DISCUSSION

With its predominantly epithelial expression, its role in epidermal immunity, and its strong links to inflammatory skin diseases ranging from AD to psoriasis,[7,10,11] it is increasingly evident that CARD14 is a major determinant of epidermal homeostasis and health. Previous studies have largely focused on the effects of CARD14-NF-κB signaling and its downstream immunological consequences in the context of skin pathology, with the current paradigm positing that elevated CARD14-NF-κB signaling promotes psoriatic diseases, while reduced signaling promotes AD.[10,11] However, the CARD14-NF-κB model alone does not fully explain the heterogeneity of CARD14-driven disease, and the broader role of CARD14 in the homeostasis of healthy skin remains unclear. In the present study, we identified

a CARD14-MYC signaling pathway that mechanistically links CARD14 to skin barrier homeostasis and helps explain the pleiotropic effects of CARD14 disease pathogenesis (Figure 7H).

Canonically, epidermal CARD14 signaling through the NF-κB and MAPK pathways form a protective antimicrobial barrier by inducing the expression of protective AMPs (e.g., S100A8, S100A9) and pro-inflammatory factors. Given this, the CARD14-NF-κB/MAPK signaling has been the primary focus of most CARD14 studies to date. However, the present study elucidates a non-canonical CARD14 signaling pathway through MYC. MYC plays a crucial role in epidermal homeostasis; its activation drives basal keratinocyte proliferation, stem cell renewal, and suprabasal keratinocyte differentiation.[12] Our data reveal a direct interaction between CARD14 and MYC and demonstrate that CARD14 activation promotes MYC dissociation, nuclear localization, and transcriptional activity. Functionally, this drives keratinocyte proliferation, suprabasal differentiation, and more robust barrier function. These findings fill a gap in the existing MYC literature, as well as prior CARD14 studies where the pro-differentiation effects of CARD14 have been noted in murine models of GoF mutations. Notably, *FLG* levels were elevated in the skin of mice expressing the *Car-d14*^{E138A} allele from birth[17] and after 1 month in a *Card14*^{E138A}-inducible model.[31] Our findings demonstrate that the regulatory effect of CARD14 on *FLG* expression that we initially described[7] is mechanistically mediated in part by CARD14-MYC signaling.

The present study establishes a paradigm that CARD14^{WT} activation regulates skin barrier function by two distinct mechanisms: (1) stimulating NF-κB to bolster the antimicrobial (chemical) barrier, and (2) stimulating MYC to bolster the physical barrier. Notably, aberrant skin function secondary to anti-microbial and/or physical epidermal dysfunction is a prominent feature of major inflammatory skin diseases, including both AD and psoriasis.[48] It is becoming clear that the association of CARD14 with both disease states arises from alterations in CARD14 signaling strength influenced by a combination of extrinsic (e.g., IL-17A) and intrinsic (e.g., missense variants) factors. The existing model posits that the risks of psoriasis and AD are increased at the high and low (including absent) extremes of CARD14-NF-κB signaling, respectively.[10,11] The CARD14-MYC pathway modifies this model by providing another direct mechanism through which CARD14 missense variants promote or potentiate inflammatory skin diseases, thereby representing a paradigm shift in how we think about CARD14-associated diseases. For example, in addition to the elevated CARD14-NF-κB signaling induced by CARD14^{E138A}, our data show increased MYC-CARD14^{E138A} dissociation compared to MYC-CARD14^{WT}, and that MYC signatures are increased in the skin of both mice and humans expressing CARD14^{E138A} compared to CARD14^{WT}. More broadly, in psoriatic skin, which typically has increased CARD14-NF-κB signaling,[30,31,42] we detected concomitantly elevated MYC signatures. We also found that, like NF-κB, MYC signals were reversed with secukinumab,[42] a biologic that reduces engagement of the CARD14-activating IL-17R[7,32] and has shown promise in treating CARD14-associated pathologies.[34,42,49] Future CARD14 studies should therefore consider not only the impact of CARD14-NF-κB signaling but also the contributions of concomitant CARD14-MYC signaling.

The CARD14-MYC pathway further complements the CARD14-NF-κB model by addressing aspects of CARD14-inflammatory skin disease not explained by either pathway alone. We found that several psoriasis-associated CARD14 mutations (e.g., R38C, H171N) that do not increase NF-κB signaling[18] still induce MYC; it is likely that CARD14-MYC signaling is one of the primary mechanisms underlying the pathogenic effects of such mutations. Conversely, we found the N737H mutation, which strongly attenuates NF-κB, does not significantly suppress MYC dissociation and function. Thus, it is possible that the effects of the N737H mutation on NF-κB drive its association with AD more so than its effects on MYC. Although the present study focused on CARD14-MYC signaling, it is probable that CARD14 and its variants modulate additional pathways than previously recognized that contribute to epithelial function and/or pathogenesis in addition to or independently from the known pathways. Future studies aimed at elucidating and describing other CARD14-driven pathways are necessary given their potential impact on human epithelial homeostasis and disease.

The CARD14-MYC pathway explains the paradoxical finding that CARD14 deficiency does not trigger severe dermatitis in mice or even humans.[10,32,35] Our data suggest that in the absence of CARD14, MYC protein remains intact and therefore capable of sustaining homeostasis of the physical barrier (even in the absence of CARD14-NF-κB signaling). This finding further supports modifications to the existing model of CARD14-driven disease by demonstrating that CARD14-MYC signaling contributes to skin homeostasis and inflammatory disease in conjunction with, but independent from, CARD14-NF-κB. The individual and combined contributions of each modality in both healthy and diseased skin warrant further scrutiny. As such, murine experiments further characterizing the mechanistic interplay between the CARD14-NF-κB and CARD14-MYC pathways under homeostatic and pathologic conditions (e.g., *Aspergillus*-induced AD) are under way in our laboratory.

We also examined the role of the CARD14-MYC pathway in other allergic diseases and epithelial tissues. Our studies uncovered downregulated MYC signatures in Th2-high asthma, eosinophilic CRwNP, and EoE, and revealed overrepresentation of the rs11652075 TT genotype in patients with EoE. These data suggest that altered CARD14-MYC signaling could affect barrier function and predispose to clinical disease in epithelia other than the epidermis, although the role of CARD14 has not been directly examined. The description of the regulation of MYC by CARD14 also raises the intriguing possibility that dysregulated CARD14-MYC signaling contributes to epithelial carcinogenesis in certain contexts. Indeed, CARD14 overexpression and upregulated nuclear MYC localization are associated with prostate cancer.[50,51] Consequently, additional studies are needed to more comprehensively examine how the CARD14-MYC pathway coordinates barrier homeostasis and disease (including cancer) within other epithelia, and how these processes are impacted by *CARD14* variants.

Our data reveal that hypomorphic CARD14 binds MYC and attenuates its activity by mediating its autophagic degradation (a notable observation given that MYC is typically degraded by the proteasome[52]). Importantly, we show that the MYC-binding small molecule 10058-F4 disrupts the interaction of MYC with CARD14. Given our finding that skin barrier function is intact when in the absence of CARD14, these data

serve as preliminary evidence that this mechanism could be leveraged therapeutically. A hypothetical agent that specifically binds CARD14 to prevent MYC binding and/or degradation could mimic CARD14-deficient conditions and thereby re-establish homeostatic MYC signaling and protective barrier function. Such an agent would be particularly beneficial in patients harboring hypomorphic CARD14 variants, which is a considerable portion of the population given the high frequency of R820W (MAF = 0.477; versus MAFs <0.0001 for the rare I593T and N737H hypomorphic mutations[11]). In summary, our findings reveal the CARD14-MYC pathway as an intracellular mechanism that could be targeted therapeutically to mitigate one's risk of inflammatory skin diseases and, more broadly, diseases characterized by epithelial barrier dysfunction.

Limitations of the study

Our study demonstrates the CARD14-MYC mechanism within keratinocytes. Although the RNA-seq analyses support that this is also the case in other epithelial cells, further studies are warranted. The primary keratinocytes used in our studies are derived from female individuals; although the cells were grown *in vitro*, results should be interpreted with this in mind. Similarly, our interpretation of CARD14 deficiency in humans is limited by only having one identified patient who is male and has a concurrent SCID; the discovery and evaluation of a heterogeneous population of patients with CARD14 deficiency is required. Our study is also limited by the number of dominant-negative and GoF variants analyzed. Future studies testing the effects of additional disease-associated variants on the CARD14-MYC mechanism are needed. Finally, the nature of the CARD14-MYC interaction and autophagy mechanism need to be studied in more detail to enable future drug-discovery experiments.

STAR★METHODS

RESOURCE AVAILABILITY

Lead contact—Further information and requests for resources and reagents should be directed to and will be fulfilled by the lead contact, Gurjit Khurana Hershey (gurjit.hershey@cchmc.org).

Materials availability—All unique reagents generated in this study are available from the lead contact with a completed materials transfer agreement.

Data and code availability

- Values underlying the statistical calculations for graphs presented within this manuscript are available in the Supplemental Information. Sequencing data are accessible in the Gene Expression Omnibus (GEO) repository[55] under the accession numbers GEO: GSE263420 and GEO: GSE263428.
- This paper does not report original code. Code utilized in this study were adapted from existing code for DESeq2,[56] EdgeR,[22] GSEA,[57] and Seurat.[58].
- Any additional information required to reanalyze the data reported in this work paper is available from the lead contact upon request.

EXPERIMENTAL MODEL AND STUDY PARTICIPANT DETAILS

MPAACH study—The recruitment details, exclusion and inclusion criteria of the MPAACH cohort have been detailed previously.[59] Briefly, enrolled participants were ≤2 years old on enrollment with a gestation of ≥36 weeks and have an AD diagnosis based on the Hanifin and Rajka criteria or the Children's Eczema Questionnaire. Exclusions include a comorbid lung condition, dependence on immunosuppression or oral steroids for a medical condition other than asthma, conditions precluding biological sample collection or spirometry, and a bleeding diathesis. Target enrollment for MPAACH (n = 700) was based on power calculations for longitudinal outcomes. Characteristics of the cohort overall and subset by analysis type are detailed in Table S1. The MPAACH study was approved by the Cincinnati Children's Hospital Medical Center (CCHMC) IRB under protocol number 2016–5842, and informed consent was provided by all subjects. Isolation of primary keratinocytes was approved by the UC IRB under protocol number 2013–4582 and determined to be non-human subjects research.

Murine model—Wild-type C57BL/6J mice were purchased from Jackson Laboratories and bred in-house. The *Card14*$^{-/-}$ mice were the kind gift of Dr. Ken Ishii (National Institutes of Biomedical Innovation, Health and Nutrition, Osaka, Japan) and were backcrossed at least eight times into the C57BL/6J background upon generation.[35] Near-equal numbers of male and female mice of each genotype ranging 2–4 months of age were utilized. Mice were maintained and handled under procedures approved by the IACUC-approved procedures at CCHMC and the Guide for the Care and Use of Laboratory Animals.[60]

Cell culture models—*In vitro* biologic studies to evaluate the variant's functionality used HaCaT keratinocytes, primary keratinocytes and fibroblasts, and HEK293T cells. Human primary keratinocytes and fibroblasts were isolated from de-identified human skin discarded from plastic surgeries in healthy females[61] at CCHMC, the University of Cincinnati (UC) and Shriners Hospital for Children-Cincinnati. Characteristics of the cell strains derived from de-identified donors are detailed in Table S4. HaCaT keratinocytes were obtained from Cell Lines Service.

METHOD DETAILS

MPAACH methods—MPAACH genotyping has been described previously.[7] Briefly, DNA from each subject was isolated from either saliva (collected using the OGR-675 kit and purified using the prepIT-L2P kit) or blood (collected in EDTA or Sodium Heparin tubes) and purified using the DNeasy Blood & Tissue Kit. DNA was subjected to genotyping using the Infinium Multi-Ethnic Global-8 Kit in the Genotyping and Sequencing Core at CCHMC.

Lesional (L) skin is defined by the Hanifin and Rajka diagnostic criteria for AD.[2] Non-lesional (NL) skin is defined as a site with no lesional history (per parental report) ≥10 cm from lesional sites. Skin tape strips were taken from L and NL skin at each MPAACH visit as described and validated previously.[59,62] 12 tape strips for each sampled skin site were collected at each visit. RNA was extracted from tapes 8 to 9 using Promega ReliaPrep RNA Miniprep System. RNA was reverse-transcribed using SuperScript IV VILO Master Mix. qPCR was performed on a LightCycler 96 instrument using TaqMan gene expression assays

and TaqMan Fast Advanced Master Mix (probes listed in the Key Resources Table) with appropriate controls as validated previously.[59,62] Expression levels were normalized to *18S* and the maximum expression from tape strip 8 and 9 from each subject is used to denote expression of each gene. Transepidermal water loss (TEWL) was assessed in non-lesional skin using the DermaLab TEWL Probe. Scoring for Atopic Dermatitis (SCORAD) was performed to assess AD severity of each subject.[63]

Murine study methods—Transepidermal water loss (TEWL) was assessed on shaved back skin using the DermaLab TEWL Probe. For histology, skin stripes were collected from the shaved area and formalin-fixed before being processed by the CCHMC Pathology Core. H&E staining and MYC immunohistochemistry were performed using standard techniques as described below. Epidermal thicknesses were measured from the H&Es using NIS Elements software.

Cell culture methods—All cells were maintained at 37°C at 5% CO_2. HaCaT keratinocytes and HEK293T cells were maintained in DMEM with low glucose, GlutaMAX supplement, and pyruvate supplemented with 10% fetal bovine serum and 1% antibiotic-antimycotic. Primary keratinocytes for ESS and ALI models were maintained in MCDB153 base media[61] supplemented with 1X antibiotic-antimycotic solution, bovine pituitary extract (2 mL/L), 0.5 μg/mL hydrocortisone, 5 μg/mL insulin, and 1 ng/mL epidermal growth factor (EGF). For experiments, primary cells were seeded into Medium 154 supplemented with human keratinocyte growth supplement (HKGS) and 1% antibiotic-antimycotic solution unless stated otherwise. Primary fibroblasts were maintained in DMEM supplemented with 1x antibiotic-antimycotic solution, 4% FBS, 0.5 μg/mL hydrocortisone, 5 μg/mL insulin, 10 ng/mL EGF, and 0.1 mM L-ascorbic acid 2-phosphate (L-AA2P).

For experiments requiring MALT1 inhibition, cells were treated with the indicated duration of mepazine prior to harvest. For experiments requiring CARD14 stimulation, cells were treated with the indicated duration of PMA and ionomycin prior to harvest. For autophagy, proteasome, mRNA stability and protein stability studies, cells were treated with 3 h bafilomycin A1 Ready Made solution, 3 h MG132, or indicated durations of actinomycin D or cycloheximide, respectively, prior to harvest. Treatment dosages are indicated in the Key Resources Table. Plasmids were transfected as required using Lipofectamine 3000. For the RNA-sequencing experiment of CARD14-GFP transfected HaCaT cells, cells were trypsinized and sorted for GFP-expressing cells by the CCHMC Research Flow Cytometry Core prior to lysis.

Plasmid cloning—The human full-length *CARD14* ORF and a synthesized FLAG-T2A sequence were restriction cloned into a pcDNA3-eGFP plasmid to generate a $CARD14^{R820W}$-FLAG-T2A-eGFP plasmid. The Q5 Site-Directed Mutagenesis (SDM) Kit was used per manufacturer's protocol to introduce modifications of interest and to remove the T2A sequence for certain applications (primers listed in the Key Resources Table). The HA-HA-MYC-mCherry plasmid was generated by restriction cloning the mCherry sequence onto the C terminus of the HA-HA-MYC construct. The CARD10–6xHis plasmid was generated by SDM-cloning a 6x-His sequence into a human *CARD10* ORF.

Plasmid sequences were confirmed by Sanger sequencing at the CCHMC Sequencing and Genotyping Core.

Air-liquid interface (ALI) and engineered skin substitute (ESS) models—For ALI experiments, $5e^5$ primary keratinocytes in Medium 154 + HKGS were seeded into 12mm Transwells (0.4 μM pore). Transwells were switched to high-calcium (1.8 mM) Medium 154 + HKGS at day 2, and lifted to ALI at day 4 (i.e., no media in top chamber). Longitudinal mepazine and 10058-F4 treatments were also initiated at day 4. Transepithelial electrical resistance (TEER) measurements were taken using an EVOM2 meter and EndOhm-12G chamber. Wells were lysed in BL buffer +1% thioglycerol for mRNA collection, radioimmunoprecipitation assay (RIPA) buffer (150 mM tris base, 150 mM NaCl, 0.1% SDS, 0.5% deoxycholate, 1% Triton X-100) with 1x Halt Protease Inhibitor Cocktail and 1x Halt Phosphatase Inhibitor Cocktail for protein collection, or formalin-fixed overnight and sectioned and stained for H&E by the CCHMC Pathology Core.

The ESS experiments were performed as previously detailed.[27] Briefly, primary fibroblasts ($5e^5$ cell/cm^2) were inoculated onto collagen-glycosaminoglycan scaffolds held at air-liquid interface with polyvinyl acetal sponges. Keratinocytes ($1e^6$ cell/cm^2) were added 24 h later and incubated for 2 weeks (37°C, 5% CO_2) on cotton pads at the air-liquid interface. For longitudinal mepazine and 10058-F4 experiments, ESS were split into separate wells and treatments applied at day 7. Culture media was comprised of DMEM/F12 which was supplemented by 0.3% FBS, 1x antibiotic-antimycotic solution, 1 mM strontium chloride, 1x insulin-transferrin-selenium solution, 10 μg/mL linoleic acid, 0.1 mM L-AA2P, 20 p.m. triiodothyronine, 0.5 μg/mL hydrocortisone, 5 ng/mL keratinocyte growth factor, and 1 ng/mL basic fibroblast growth factor. ESS biopsies were formalin-fixed overnight and sectioned by the CCHMC Pathology Core. PLAs were performed as noted below.

Quantitative PCR—HaCaT cells were seeded into 12-well plates in complete media and treatment initiated the following day. Cells were lysed in BL buffer +1% thioglycerol, RNA isolated using the ReliaPrep RNA Miniprep System, and reverse-transcribed using SuperScript IV VILO Master Mix. For qPCR analysis, the resulting cDNA was run on the QuantStudio 3 Real-Time PCR System using TaqMan Fast Advanced Master Mix and TaqMan probes per manufacturer's instructions. Ct values for analysis were obtained from Applied Biosystems Analysis Software and further analyzed in Microsoft Excel.

RNA-sequencing—The untransfected biological replicates submitted to the UC Genomics, Epigenomics and Sequencing Core[64] were checked for quality control and subjected to bulk RNA-sequencing (1×85bp) using the Illumina NextSeq 550 System. Quality trimmed reads were mapped to the human hg19 genome, quantified using RSEM[65] and mapped with Bowtie 2[66] using default thresholds within the computational suite for bioinformaticians and biologists tool (CSBB v. 3). Resulting counts matrices were analyzed in R using the DESeq2[56] and EdgeR[22] packages to generate differential expression data, and GSEA was performed using the fgsea package[57] in R. Differentially expressed genes were also examined by Ingenuity Pathway Analysis software and by iLINCS.[20] The workflow for the CARD14-GFP-transfected HaCaT experiment was similar but utilized the NEBNext

Single Cell/Low Input RNA Library Prep Kit and was sequenced with a PE 2×61bp setting on an Illumina NextSeq 2000 System.

Immunoprecipitations (IPs), immunoblotting—HaCaT keratinocytes were plated and either treated or transfected (using Lipofectamine 3000) the next day as required. Except for cell fractionation experiments, cells were lysed in RIPA buffer with protease and phosphatase inhibitors for immunoblots.

For cell fractionation, cells were scraped, pelleted, and resuspended in 400 μL CE buffer (10 mM HEPES; 10 mM KCl, 0.1 mM EDTA, 1mM DTT, protease and phosphatase inhibitors). 25 μL of 10% NP-40 was added. After centrifugation, the supernatant (cytoplasmic fraction) was removed. The nuclear fraction was washed with PBS and lysed in 30 μL of NE buffer (20 mM HEPES, 0.4 M NaCl, 1 mM EDTA, 1 mM DTT, protease and phosphatase inhibitors). Samples were subjected to immunoblotting as described below.

For IPs, 50 μL lysate was incubated overnight with 1 μg antibody with rotation at 4°C. Antibody-protein complexes were incubated 1 h with Protein G Dynabeads, IP'd with a magnetic rack and washed with wash buffer (20 mM Tris base pH 7.5, 150 mM NaCl, 1 mM EDTA, 1 mM EGTA, 1% Triton X-100, 1 mM Na_3VO_4, 0.1% SDS). Proteins were eluted by boiling 10 min at 95°C in 12 μL 6x sample buffer (60 mM Tris base pH 6.8, 12% SDS, 47% glycerol, 10% β-mercaptoethanol, bromophenol blue). As loading control, 5 μL of original lysate was also prepared in 6x sample buffer. Samples were run as described below.

For all immunoblots, samples concentrations were determined using the Pierce BCA Protein Assay Kit. Equal amounts of protein were prepared in 6x sample buffer and run on either 10- or 15-well 4–15% Mini-PROTEAN TGX Precast Protein Gels with in Tris/Glycine/SDS running buffer for 40 min at 200 V, then transferred to an Immun-Blot PVDF membrane in Tris/Glycine Buffer for 60 min at 100 V. Blots were blocked for 1 h in EveryBlot Blocking Buffer, incubated with primary antibody overnight, and with secondary antibodies for 1 h prior to imaging with Immobilon Forte Western HRP Substrate on the ChemiDoc MP Imaging System. Where appropriate, blots were stripped 10 min with Restore PLUS Western Blot Stripping Buffer. Densitometry was performed using Image Lab 6.1 software. Target gene band intensities were normalized to the respective housekeeping band intensities. Autophagic flux was calculated by dividing the normalized intensities of bafilomycin-treated samples by the normalized intensities of the corresponding vehicle-treated samples. Antibodies and concentrations used are listed in the Key Resources Table.

Imaging—For nuclear MYC immunofluorescent (IF) experiments, HaCaT keratinocytes were seeded into wells containing gelatin-coated coverslips and treated with mepazine or vehicle for 24 h prior to formalin fixation. Cells were permeabilized in PBS +0.25% Triton X-, blocked 1 h in 5% normal donkey serum (NDS), incubated with MYC antibody overnight, and with secondary antibody 1 h. Nuclei were counterstained with DAPI (1:000) before mounting onto slides with ProLong Diamond Antifade Mountant. Images were obtained with identical settings on a Nikon A1 LUNV inverted microscope in the CCHMC Bio-Imaging and Analysis Facility, and nuclear MYC intensity quantified using ImageJ using the StarDist plugin.

For proximity ligation assays (PLAs), KO HaCaT cells were seeded into gelatin-coated 8-well Ibidi slides with removable wells. The following day, cells were transfected with plasmids and/or treated as indicated prior to formalin fixation and permeabilization (as above). For ESS PLAs, paraffin-embedded ESS sections were deparaffinized and subjected to heat-induced epitope retrieval with sodium citrate. All slides were treated in accordance with the NaveniFlex MR PLA kit per the manufacturer's protocol. Nuclei were counterstained with DAPI (1:1000) before coverslipping with ProLong Diamond Antifade Mountant. Images were obtained with identical settings on a Nikon A1 LUNV inverted microscope in the CCHMC Bio-Imaging and Analysis Facility. Puncta were counted in R5 HaCaT keratinocytes that were found to be co-transfected with the desired construct(s).

For mitochondrial imaging, HaCaT cells were seeded into 8-well Ibidi slides for 48 h, then stained with tetramethylrhodamine, ethyl ester (TMRE), Acridine Orange 10-Nonyl Bromide (NAO), and NucRed Live 647 for 30 min prior to live-cell imaging on a Nikon A1R inverted LUNV confocal microscope. z stack images were processed and analyzed for staining intensity in NIS Elements and IMARIS software.

Proliferation & migration assays

Cell Trace Violet proliferation and Ki67 flow Cytometry: HaCaT keratinocytes were seeded into 6-well plates and the next day stained with Cell Trace Violet per manufacturer's protocol before treatment with DMSO (vehicle) or mepazine. Media and treatments were changed daily. After 72 h, cells were trypsinized, stained with the LIVE/DEAD Fixable Near-IR Dead Cell Stain Kit, and fixed and permeabilized with IC Fixation Buffer and Permeabilization Buffers, respectively. Cells were stained with Ki67-BUV737 for 30 min before analysis on a BD LSRFortessa Cell Analyzer in the CCHMC Research Flow Cytometry Core. Data were analyzed on FlowJo, using single-stained controls for compensation.

WST-1 Colorimetric proliferation assay: HaCaT keratinocytes were seeded into 96-well plates. At each time point, 100 μL of media with 10 μL WST-1 Assay Reagent for and incubated 2 h before reading on an Agilent BioTek Microplate Reader. Final values were calculated by subtracting background (650 nM) from signal (440 nM) readings.

Wound Healing "Scratch" Assay: HaCaTs were seeded into 24-well plates and grown to confluence. After 48 h, wells were treated for 3hr with Mitomycin C, after which a scratch was created with a p200 pipette tip and mepazine or vehicle treatment. At 0 and 24 h, images of the same location in each well were obtained using a Zeiss AxioCam ERc5s camera mounted on an Axio Vert A1 microscope using Zen 3.3 Blue software. Scratch wound areas were quantified in ImageJ, and % closure calculated for each well as ($Area_{24hr}$/$Area_{0hr}$)*100%.

Seahorse: HaCaT keratinocytes were seeded in complete media into a Seahorse XF96 cell culture microplates and media changed after 3 h. Media was switched to XF DMEM after 24 h and cells were subjected to the Seahorse XF Real-Time ATP Rate Assay per

manufacturer's protocol on a Seahorse XFe96 Analyzer instrument. Data was exported and analyzed using the Agilent Seahorse Analytics software.

***In silico* analyses:** Clustal O (1.2.4) was used to align the UniProt CARD14 amino acid sequence (UniProt: Q9BXL6) to its homologous proteins in several mammalian species. Predicted structural and/or functional consequences of the R820W variant were tested by the *in silico* algorithms PolyPhen2,[13] SIFT,[14] SNAP2[15] and SuSPect.[16] Structural modeling of the complex between the C-terminal helical region of MYC (residues 349–439) and the MAGUK region of CARD14 (residues 569–1000) was performed using AlphaFold Multimer[67,68] with Amber force field relaxation via the Google Research Colaboratory. Previously-published RNA-sequencing and microarray data were obtained from the GEO repository (Table S5). For human studies, rs11652075 genotypes were determined in RNAseq datasets by counting the number of FASTQ reads aligning to the rs11652075 C- or T-allele in Python, then assigning a call based on the following criteria: if (≥8 C & 0 T) or (C > 8 & C/T > 5) = *CARD14* $^{C/C}$; if (0C& ≥8 T) or (T > 8 & T/C > 5) = CARD14 $^{T/T}$; if (C > 8 & T > 8) or (not *CARD14* $^{C/C}$ & not *CARD14* $^{T/T}$ & (C + T > 8) & (C/T < 5 or T/C < 5)) = *CARD14* $^{C/T}$. If untransformed count matrices were available, data was analyzed in R using DESeq2 and GSEA as above. If such matrices were unavailable, differential expression analysis was determined using the GEO2R tool[18] if available before GSEA analysis in R. If neither were available, raw counts matrices were rederived from deposited FASTQ files as above. The single cell RNA-seq dataset from GEO: GSE147482 was analyzed using Seurat[58] in R.

QUANTIFICATION AND STATISTICAL ANALYSIS

For all data statistics were performed on non-normalized data with $\alpha = 0.05$ unless otherwise noted. This non-normalized data is provided in the supplemental information. For MPAACH data, distributional characteristics of all continuous variables were evaluated for normality following log-transformation and associations between the indicated rs11652075 genotype groups and the designated outcomes were performed using generalized linear modeling in R, specifically using linear regression with the identity link function within the Gaussian family. Unless otherwise noted, all other experiments were performed at least three independent times (with exact replicate numbers noted in the figure legends) and their statistics performed in GraphPad Prism 9. Distributional characteristics of all continuous variables were evaluated for normality following log-transformation when required and statistical analyses were performed with two-tailed parametric or non-parametric tests accordingly. When shown, Tukey's post-hoc tests were utilized in ANOVA analyses. For qPCR analyses, fold change expression in each condition was calculated by the $2^{-\Delta\Delta CT}$ method.[69] WST-1 proliferation doubling times were determined by exponential regression modeling, and both MYC and MAD protein and mRNA half-lives were determined using one-phase decay regression modeling. Maximum ALI TEER values were determined using Gaussian nonlinear regression modeling.

Supplementary Material

Refer to Web version on PubMed Central for supplementary material.

ACKNOWLEDGMENTS

S.B.D., D.E.O., A.B.H., J.M.B., L.J.M., and G.K.K.H. disclose support for the research of this work from the National Institutes of Health (U19AI70235, T32GM063483, R01AI162964, and T32ES010957). We thank Brittany Grashel, Seth Jenkins, David Morgan, and Daniel Spagna for technical assistance. We thank the participating MPAACH children and families, as well as the staff who work on the MPAACH study. We thank the laboratories who generously provided plasmids through Addgene, as listed in the key resources table. This publication was also made possible, in part, using the Cincinnati Children's Research Flow Cytometry Facility (RRID: SCR_022635), Bio-Imaging and Analysis Facility (RRID: SCR_022628), Integrated Pathology Research Facility (RRID: SCR_022637), and Genomics Sequencing Facility (RRID: SCR_022630), as well as the University of Cincinnati Genomics, Epigenomics, and Sequencing Core. Several figure panels and the graphical abstract were generated using BioRender.

REFERENCES

1. Davidson WF, Leung DYM, Beck LA, Berin CM, Boguniewicz M, Busse WW, Chatila TA, Geha RS, Gern JE, Guttman-Yassky E, et al. (2019). Report from the National Institute of Allergy and Infectious Diseases workshop on "Atopic dermatitis and the atopic march: Mechanisms and interventions.". J. Allergy Clin. Immunol 143, 894–913. 10.1016/j.jaci.2019.01.003. [PubMed: 30639346]
2. Yazici D, Ogulur I, Kucukkase O, Li M, Rinaldi AO, Pat Y, Wallimann A, Wawrocki S, Celebi Sozener Z, Buyuktiryaki B, et al. (2022). Epithelial barrier hypothesis and the development of allergic and autoimmune diseases. Allergo J. Int 31, 91–102. 10.1007/s40629-022-00211-y.
3. Montero-Vilchez T, Segura-Fernández-Nogueras M-V, Pérez-Rodríguez I, Soler-Gongora M, Martinez-Lopez A, Fernández-González A, Molina-Leyva A, and Arias-Santiago S (2021). Skin Barrier Function in Psoriasis and Atopic Dermatitis: Transepidermal Water Loss and Temperature as Useful Tools to Assess Disease Severity. J. Clin. Med 10, 359. 10.3390/jcm10020359. [PubMed: 33477944]
4. Moreci RS, and Lechler T (2020). Epidermal structure and differentiation. Curr. Biol 30, R144–R149. 10.1016/j.cub.2020.01.004. [PubMed: 32097634]
5. Drislane C, and Irvine AD (2020). The role of filaggrin in atopic dermatitis and allergic disease. Ann. Allergy Asthma Immunol 124, 36–43. 10.1016/j.anai.2019.10.008. [PubMed: 31622670]
6. Kezic S, and Jakasa I (2016). Filaggrin and Skin Barrier Function. Curr. Probl. Dermatol 49, 1–7. 10.1159/000441539. [PubMed: 26844893]
7. DeVore SB, Stevens ML, He H, Biagini JM, Kroner JW, Martin LJ, and Khurana Hershey GK (2022). Novel Role for Caspase Recruitment Domain Family Member 14 and its Genetic Variant rs11652075 in Skin Filaggrin Homeostasis. J. Allergy Clin. Immunol 149, 708–717. 10.1016/j.jaci.2021.07.003. [PubMed: 34271060]
8. Consortium GTEx (2013). The Genotype-Tissue Expression (GTEx) project. Nat. Genet 45, 580–585. 10.1038/ng.2653. [PubMed: 23715323]
9. DeVore SB, and Khurana Hershey GK (2022). The role of the CBM complex in allergic inflammation and disease. J. Allergy Clin. Immunol 150, 1011–1030. 10.1016/j.jaci.2022.06.023. [PubMed: 35981904]
10. Mellett M (2020). Regulation and dysregulation of CARD14 signalling and its physiological consequences in inflammatory skin disease. Cell. Immunol 354, 104147. 10.1016/j.cellimm.2020.104147. [PubMed: 32593012]
11. Peled A, Sarig O, Sun G, Samuelov L, Ma CA, Zhang Y, Dimaggio T, Nelson CG, Stone KD, Freeman AF, et al. (2019). Loss-of-function mutations in caspase recruitment domain-containing protein 14 (CARD14) are associated with a severe variant of atopic dermatitis. J. Allergy Clin. Immunol 143, 173–181.e10. 10.1016/j.jaci.2018.09.002. [PubMed: 30248356]
12. Watt FM, Frye M, and Benitah SA (2008). MYC in mammalian epidermis: how can an oncogene stimulate differentiation? Nat. Rev. Cancer 8, 234–242. 10.1038/nrc2328. [PubMed: 18292777]
13. Adzhubei IA, Schmidt S, Peshkin L, Ramensky VE, Gerasimova A, Bork P, Kondrashov AS, and Sunyaev SR (2010). A method and server for predicting damaging missense mutations. Nat. Methods 7, 248–249. 10.1038/nmeth0410-248. [PubMed: 20354512]

14. Kumar P, Henikoff S, and Ng PC (2009). Predicting the effects of coding non-synonymous variants on protein function using the SIFT algorithm. Nat. Protoc 4, 1073–1081. 10.1038/nprot.2009.86. [PubMed: 19561590]
15. Hecht M, Bromberg Y, and Rost B (2015). Better prediction of functional effects for sequence variants. BMC Genom 16, 1–12. 10.1186/1471-2164-16-S8-S1.
16. Yates CM, Filippis I, Kelley LA, and Sternberg MJE (2014). SuSPect: Enhanced Prediction of Single Amino Acid Variant (SAV) Phenotype Using Network Features. J. Mol. Biol 426, 2692–2701. 10.1016/j.jmb.2014.04.026. [PubMed: 24810707]
17. Mellett M, Meier B, Mohanan D, Schairer R, Cheng P, Satoh TK, Kiefer B, Ospelt C, Nobbe S, Thome M, et al. (2018). CARD14 Gain-of-Function Mutation Alone Is Sufficient to Drive IL-23/IL-17–Mediated Psoriasiform Skin Inflammation In Vivo. J. Invest. Dermatol 138, 2010–2023. 10.1016/j.jid.2018.03.1525. [PubMed: 29689250]
18. Jordan CT, Cao L, Roberson EDO, Duan S, Helms CA, Nair RP, Duffin KC, Stuart PE, Goldgar D, Hayashi G, et al. (2012). Rare and Common Variants in CARD14, Encoding an Epidermal Regulator of NF-kappaB, in Psoriasis. Am. J. Hum. Genet 90, 796–808. 10.1016/j.ajhg.2012.03.013. [PubMed: 22521419]
19. Conacci-Sorrell M, McFerrin L, and Eisenman RN (2014). An Overview of MYC and Its Interactome. Cold Spring Harb. Perspect. Med 4, a014357. 10.1101/cshperspect.a014357. [PubMed: 24384812]
20. Pilarczyk M, Fazel-Najafabadi M, Kouril M, Shamsaei B, Vasiliauskas J, Niu W, Mahi N, Zhang L, Clark NA, Ren Y, et al. (2022). Connecting omics signatures and revealing biological mechanisms with iLINCS. Nat. Commun 13, 4678. 10.1038/s41467-022-32205-3. [PubMed: 35945222]
21. Farrell AS, and Sears RC (2014). MYC Degradation. Cold Spring Harb. Perspect. Med 4, a014365. 10.1101/cshperspect.a014365. [PubMed: 24591536]
22. Robinson MD, McCarthy DJ, and Smyth GK (2010). edgeR: a Bio-conductor package for differential expression analysis of digital gene expression data. Bioinformatics 26, 139–140. 10.1093/bio-informatics/btp616. [PubMed: 19910308]
23. Rosenbaum M, Schnalzger T, Engleitner T, Weiß C, Mishra R, Mibus C, Mitterer T, Rad R, and Ruland J (2022). MALT1 protease function in regulatory T cells induces MYC activity to promote mitochondrial function and cellular expansion. Eur. J. Immunol 52, 85–95. 10.1002/eji.202149355. [PubMed: 34668583]
24. Otręba M, Stojko J, and Rzepecka-Stojko A (2023). The role of phenothiazine derivatives in autophagy regulation: A systematic review. J. Appl. Toxicol 43, 474–489. 10.1002/jat.4397. [PubMed: 36165981]
25. Israël L, Bardet M, Huppertz A, Mercado N, Ginster S, Unterreiner A, Schlierf A, Goetschy JF, Zerwes H-G, Roth L, et al. (2018). A CARD10-Dependent Tonic Signalosome Activates MALT1 Paracaspase and Regulates IL-17/TNF-a–Driven Keratinocyte Inflammation. J. Invest. Dermatol 138, 2075–2079. 10.1016/j.jid.2018.03.1503. [PubMed: 29571942]
26. Hegazy M, Cohen-Barak E, Koetsier JL, Najor NA, Arvanitis C, Sprecher E, Green KJ, and Godsel LM (2020). Proximity Ligation Assay for Detecting Protein-Protein Interactions and Protein Modifications in Cells and Tissues In Situ. Curr. Protoc. Cell Biol 89, e115. 10.1002/cpcb.115. [PubMed: 33044803]
27. Supp DM, Hahn JM, Lloyd CM, Combs KA, Swope VB, Abdel-Malek Z, and Boyce ST (2020). Light or Dark Pigmentation of Engineered Skin Substitutes Containing Melanocytes Protects Against Ultraviolet Light-Induced DNA Damage In Vivo. J. Burn Care Res 41, 751–760. 10.1093/jbcr/iraa029. [PubMed: 32052834]
28. Danne C, Michaudel C, Skerniskyte J, Planchais J, Magniez A, Agus A, Michel M-L, Lamas B, Da Costa G, Spatz M, et al. (2023). CARD9 in neutrophils protects from colitis and controls mitochondrial metabolism and cell survival. Gut 72, 1081–1092. 10.1136/gutjnl-2022-326917. [PubMed: 36167663]
29. Wang S, Drummond ML, Guerrero-Juarez CF, Tarapore E, MacLean AL, Stabell AR, Wu SC, Gutierrez G, That BT, Benavente CA, et al. (2020). Single cell transcriptomics of human epidermis identifies basal stem cell transition states. Nat. Commun 11, 4239. 10.1038/s41467-020-18075-7. [PubMed: 32843640]

30. Jordan CT, Cao L, Roberson EDO, Pierson KC, Yang C-F, Joyce CE, Ryan C, Duan S, Helms CA, Liu Y, et al. (2012). PSORS2 is due to mutations in CARD14. Am. J. Hum. Genet 90, 784–795. 10.1016/j.ajhg.2012.03.012. [PubMed: 22521418]

31. Manils J, Webb LV, Howes A, Janzen J, Boeing S, Bowcock AM, and Ley SC (2020). CARD14E138A signalling in keratinocytes induces TNF-dependent skin and systemic inflammation. Elife 9, e56720. 10.7554/eLife.56720. [PubMed: 32597759]

32. Wang M, Zhang S, Zheng G, Huang J, Songyang Z, Zhao X, and Lin X (2018). Gain-of-Function Mutation of Card14 Leads to Spontaneous Psoriasis-like Skin Inflammation through Enhanced Keratinocyte Response to IL-17A. Immunity 49, 66–79.e5. 10.1016/j.im-muni.2018.05.012. [PubMed: 29980436]

33. Van Nuffel E, Schmitt A, Afonina IS, Schulze-Osthoff K, Beyaert R, and Hailfinger S (2017). CARD14-Mediated Activation of Paracaspase MALT1 in Keratinocytes: Implications for Psoriasis. J. Invest. Dermatol 137, 569–575. 10.1016/j.jid.2016.09.031. [PubMed: 27939769]

34. Dai S, Zhang S, Wang C, Lin X, and Lin Z (2023). CARD14 Missense Variant Underlying CARD14-Associated Papulosquamous Eruption with Beneficial Response to Secukinumab. JID Innov 3, 100174. 10.1016/j.xjidi.2022.100174. [PubMed: 36699196]

35. Tanaka M, Kobiyama K, Honda T, Uchio-Yamada K, Natsume-Kitatani Y, Mizuguchi K, Kabashima K, and Ishii KJ (2018). Essential Role of CARD14 in Murine Experimental Psoriasis. J. Immunol 200, 71–81. 10.4049/jimmunol.1700995. [PubMed: 29150564]

36. Cirillo E, Cancrini C, Azzari C, Martino S, Martire B, Pession A, Tommasini A, Naviglio S, Finocchi A, Consolini R, et al. (2019). Clinical, Immunological, and Molecular Features of Typical and Atypical Severe Combined Immunodeficiency: Report of the Italian Primary Immunodeficiency Network. Front. Immunol 10, 1908. [PubMed: 31456805]

37. Tennessen JA, Bigham AW, O'Connor TD, Fu W, Kenny EE, Gravel S, McGee S, Do R, Liu X, Jun G, et al. (2012). Evolution and functional impact of rare coding variation from deep sequencing of human exomes. Science 337, 64–69. 10.1126/science.1219240. [PubMed: 22604720]

38. Saleheen D, Natarajan P, Armean IM, Zhao W, Rasheed A, Khetarpal SA, Won H-H, Karczewski KJ, O'Donnell-Luria AH, Samocha KE, et al. (2017). Human knockouts and phenotypic analysis in a cohort with a high rate of consanguinity. Nature 544, 235–239. 10.1038/nature22034. [PubMed: 28406212]

39. Karczewski KJ, Francioli LC, Tiao G, Cummings BB, Alföldi J, Wang Q, Collins RL, Laricchia KM, Ganna A, Birnbaum DP, et al. (2020). The mutational constraint spectrum quantified from variation in 141,456 humans. Nature 581, 434–443. 10.1038/s41586-020-2308-7. [PubMed: 32461654]

40. Li B, Tsoi LC, Swindell WR, Gudjonsson JE, Tejasvi T, Johnston A, Ding J, Stuart PE, Xing X, Kochkodan JJ, et al. (2014). Transcriptome analysis of psoriasis in a large case-control sample: RNA-seq provides insights into disease mechanisms. J. Invest. Dermatol 134, 1828–1838. 10.1038/jid.2014.28. [PubMed: 24441097]

41. Israel L, and Mellett M (2018). Clinical and Genetic Heterogeneity of CARD14 Mutations in Psoriatic Skin Disease. Front. Immunol 9, 2239. 10.3389/fimmu.2018.02239. [PubMed: 30386326]

42. Liu J, Chang H-W, Grewal R, Cummins DD, Bui A, Beck KM, Sekhon S, Yan D, Huang Z-M, Schmidt TH, et al. (2022). Transcriptomic Profiling of Plaque Psoriasis and Cutaneous T-Cell Subsets during Treatment with Secukinumab. JID Innov 2, 100094. 10.1016/j.xjidi.2021.100094. [PubMed: 35757784]

43. Shi G, Li SJ, Wang TT, Cheng CM, Fan YM, and Zhu KJ (2016). The common CARD14 gene missense polymorphism rs11652075 (c.C2458T/p.Arg820Trp) is associated with psoriasis: a meta-analysis. Genet. Mol. Res 15, 10–4238. 10.4238/gmr.15038357.

44. Greuter T, Straumann A, Fernandez-Marrero Y, Germic N, Hosseini A, Yousefi S, Simon D, Collins MH, Bussmann C, Chehade M, et al. (2022). Characterization of eosinophilic esophagitis variants by clinical, histological, and molecular analyses: A cross-sectional multi-center study. Allergy 77, 2520–2533. 10.1111/all.15233. [PubMed: 35094416]

45. Hill DA, and Spergel JM (2018). Is eosinophilic esophagitis a member of the atopic march? Ann. Allergy Asthma Immunol 120, 113–114. 10.1016/j.anai.2017.10.003. [PubMed: 29413330]

46. Christenson SA, Steiling K, van den Berge M, Hijazi K, Hiemstra PS, Postma DS, Lenburg ME, Spira A, and Woodruff PG (2015). Asthma–COPD Overlap. Clinical Relevance of Genomic Signatures of Type 2 Inflammation in Chronic Obstructive Pulmonary Disease. Am. J. Respir. Crit. Care Med 191, 758–766. 10.1164/rccm.201408-1458OC. [PubMed: 25611785]
47. Wang W, Gao Z, Wang H, Li T, He W, Lv W, and Zhang J (2016). Transcriptome Analysis Reveals Distinct Gene Expression Profiles in Eosinophilic and Noneosinophilic Chronic Rhinosinusitis with Nasal Polyps. Sci. Rep 6, 26604. 10.1038/srep26604. [PubMed: 27216292]
48. Guttman-Yassky E, Nograles KE, and Krueger JG (2011). Contrasting pathogenesis of atopic dermatitis and psoriasis—Part I: Clinical and pathologic concepts. J. Allergy Clin. Immunol 127, 1110–1118. 10.1016/j.jaci.2011.01.053. [PubMed: 21388665]
49. López-Sánchez C, Falla LM, Roé-Crespo E, Arostegui JI, Mozos A, Bernal S, Iznardo H, and Baselga-Torres E (2021). Excellent response to secukinumab in an infant with severe generalized pustular psoriasis. J. Dermatol 48, 907–910. 10.1111/1346-8138.15673. [PubMed: 33543522]
50. Vanneste D, Staal J, Haegman M, Driege Y, Carels M, Van Nuffel E, De Bleser P, Saeys Y, Beyaert R, and Afonina IS (2022). CARD14 Signalling Ensures Cell Survival and Cancer Associated Gene Expression in Prostate Cancer Cells. Biomedicines 10, 2008. 10.3390/biomedicines10082008. [PubMed: 36009554]
51. Gurel B, Iwata T, Koh CM, Jenkins RB, Lan F, Van Dang C, Hicks JL, Morgan J, Cornish TC, Sutcliffe S, et al. (2008). Nuclear MYC protein overexpression is an early alteration in human prostate carcinogenesis. Mod. Pathol 21, 1156–1167. 10.1038/modpathol.2008.111. [PubMed: 18567993]
52. Ahmadi SE, Rahimi S, Zarandi B, Chegeni R, and Safa M (2021). MYC: a multipurpose oncogene with prognostic and therapeutic implications in blood malignancies. J. Hematol. Oncol 14, 121. 10.1186/s13045-021-01111-4. [PubMed: 34372899]
53. Vo BT, Wolf E, Kawauchi D, Gebhardt A, Rehg JE, Finkelstein D, Walz S, Murphy BL, Youn YH, Han Y-G, et al. (2016). The Interaction of Myc with Miz1 Defines Medulloblastoma Subgroup Identity. Cancer Cell 29, 5–16. 10.1016/j.ccell.2015.12.003. [PubMed: 26766587]
54. Schmid-Burgk JL, Höning K, Ebert TS, and Hornung V (2016). CRISPaint allows modular base-specific gene tagging using a ligase-4-dependent mechanism. Nat. Commun 7, 12338. 10.1038/ncomms12338. [PubMed: 27465542]
55. Edgar R, Domrachev M, and Lash AE (2002). Gene Expression Omnibus: NCBI gene expression and hybridization array data repository. Nucleic Acids Res 30, 207–210. 10.1093/nar/30.1.207. [PubMed: 11752295]
56. Love MI, Huber W, and Anders S (2014). Moderated estimation of fold change and dispersion for RNA-seq data with DESeq2. Genome Biol 15, 550. 10.1186/s13059-014-0550-8. [PubMed: 25516281]
57. Korotkevich G, Sukhov V, Budin N, Shpak B, Artyomov MN, and Sergushichev A (2016). Fast gene set enrichment analysis. Preprint at bioRxiv, 060012. 10.1101/060012.
58. Hao Y, Hao S, Andersen-Nissen E, Mauck WM, Zheng S, Butler A, Lee MJ, Wilk AJ, Darby C, Zager M, et al. (2021). Integrated analysis of multimodal single-cell data. Cell 184, 3573–3587.e29. 10.1016/j.cell.2021.04.048. [PubMed: 34062119]
59. Biagini Myers JM, Sherenian MG, Baatyrbek kyzy A, Alarcon R, An A, Flege Z, Morgan D, Gonzalez T, Stevens ML, He H, et al. (2020). Events in Normal Skin Promote Early-life Atopic Dermatitis - the MPAACH Cohort. J. Allergy Clin. Immunol. Pract 8, 2285–2293.e6. 10.1016/j.jaip.2020.03.048. [PubMed: 32302785]
60. National Research Council (US) (2011). Committee for the Update of the Guide for theCare and Use of Laboratory Animals. Guide for the Care and Use of Laboratory Animals, 8th ed. (National Academies Press).
61. Supp DM, Hahn JM, Combs KA, McFarland KL, and Powell HM (2022). Isolation and feeder-free primary culture of four cell types from a single human skin sample. STAR Protoc 3, 101172. 10.1016/j.xpro.2022.101172. [PubMed: 35199036]
62. Stevens ML, Gonzalez T, Schauberger E, Baatyrbek kyzy A, Andersen H, Spagna D, Kalra MK, Martin LJ, Haslam D, Herr AB, et al. (2020). Simultaneous skin biome and keratinocyte genomic

capture reveals microbiome differences by depth of sampling. J. Allergy Clin. Immunol 146, 1442–1445. 10.1016/j.jaci.2020.04.004. [PubMed: 32320735]

63. Schallreuter KU, Levenig C, Berger J, Umbert J, Winkelmann RK, Wegener L, Correia O, Chosidow O, Saiag P, Bastuji-Garin S, et al. (1993). Severity Scoring of Atopic Dermatitis: The SCORAD Index. Dermatology 186, 23–31. 10.1159/000247298. [PubMed: 8435513]
64. Qiu K, Zou W, Fang Z, Wang Y, Bell S, Zhang X, Tian Z, Xu X, Ji B, Li D, et al. (2023). 2D MoS2 and BN Nanosheets Damage Mitochondria through Membrane Penetration. ACS Nano 17, 4716–4728. 10.1021/acsnano.2c11003. [PubMed: 36848459]
65. Li B, and Dewey CN (2011). RSEM: accurate transcript quantification from RNA-Seq data with or without a reference genome. BMC Bioinf 12, 323. 10.1186/1471-2105-12-323.
66. Langmead B, and Salzberg SL (2012). Fast gapped-read alignment with Bowtie 2. Nat. Methods 9, 357–359. 10.1038/nmeth.1923. [PubMed: 22388286]
67. Evans R, O'Neill M, Pritzel A, Antropova N, Senior A, Green T, Žídek A, Bates R, Blackwell S, Yim J, et al. (2022). Protein complex prediction with AlphaFold-Multimer. Preprint at bioRxiv. 10.1101/2021.10.04.463034.
68. Jumper J, Evans R, Pritzel A, Green T, Figurnov M, Ronneberger O, Tunyasuvunakool K, Bates R, Žídek A, Potapenko A, et al. (2021). Highly accurate protein structure prediction with AlphaFold. Nature 596, 583–589. 10.1038/s41586-021-03819-2. [PubMed: 34265844]
69. Livak KJ, and Schmittgen TD (2001). Analysis of relative gene expression data using real-time quantitative PCR and the 2(-Delta Delta C(T)) Method. Methods San Diego Calif 25, 402–408. 10.1006/meth.2001.1262. [PubMed: 11846609]

Highlights

- CARD14 signaling directly regulates MYC in keratinocytes to promote barrier homeostasis
- Pathogenic genetic variants dysregulate CARD14-MYC signaling, promoting barrier dysfunction
- Skin barrier function remains intact in the context of complete CARD14 deficiency
- The CARD14-MYC mechanism may contribute to diseases beyond the epidermis

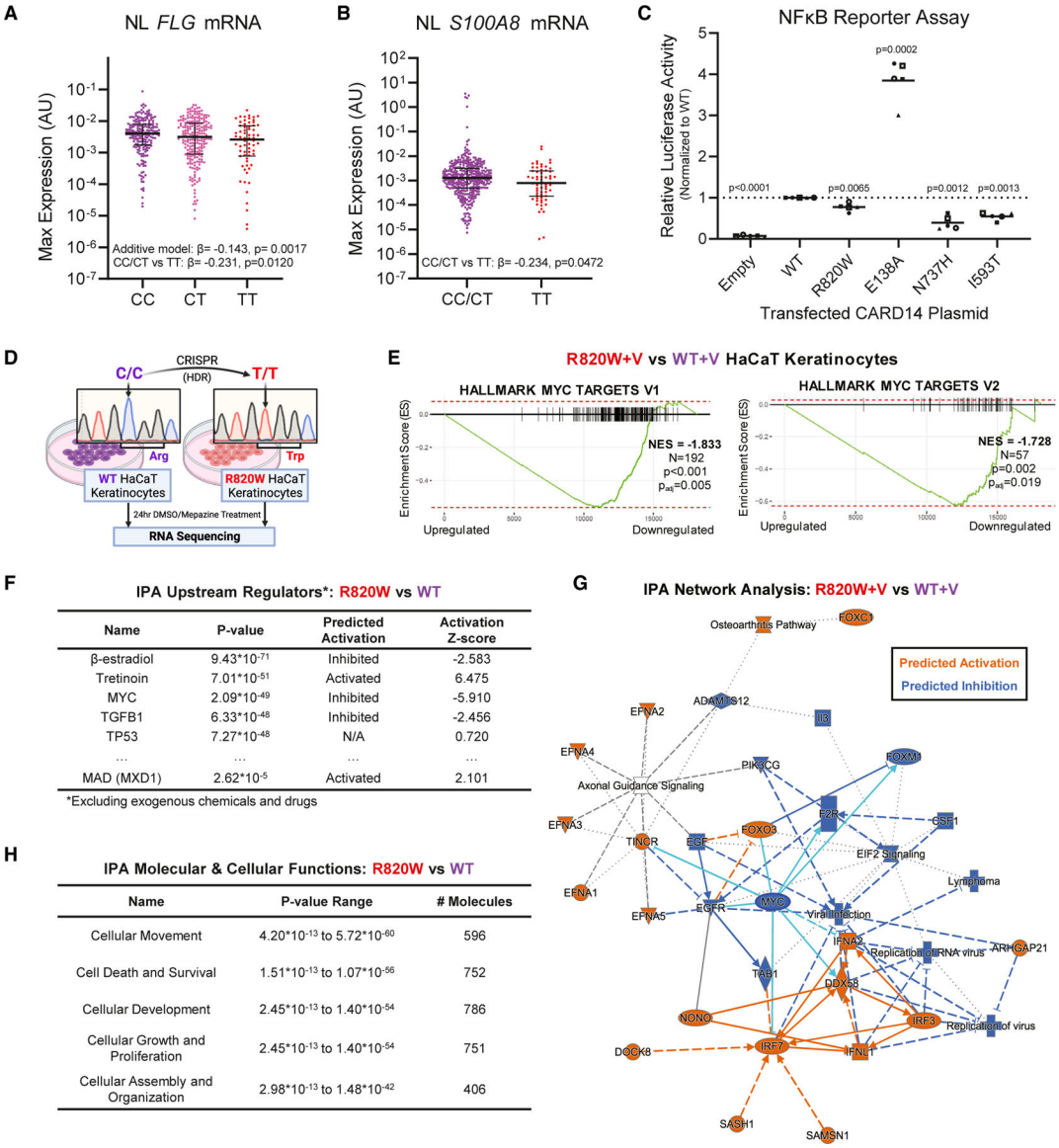

Name	P-value	Predicted Activation	Activation Z-score
β-estradiol	$9.43*10^{-71}$	Inhibited	-2.583
Tretinoin	$7.01*10^{-51}$	Activated	6.475
MYC	$2.09*10^{-49}$	Inhibited	-5.910
TGFB1	$6.33*10^{-48}$	Inhibited	-2.456
TP53	$7.27*10^{-48}$	N/A	0.720
…	…	…	…
MAD (MXD1)	$2.62*10^{-5}$	Activated	2.101

*Excluding exogenous chemicals and drugs

Name	P-value Range	# Molecules
Cellular Movement	$4.20*10^{-13}$ to $5.72*10^{-60}$	596
Cell Death and Survival	$1.51*10^{-13}$ to $1.07*10^{-56}$	752
Cellular Development	$2.45*10^{-13}$ to $1.40*10^{-54}$	786
Cellular Growth and Proliferation	$2.45*10^{-13}$ to $1.40*10^{-54}$	751
Cellular Assembly and Organization	$2.98*10^{-13}$ to $1.48*10^{-42}$	406

Figure 1. The AD-associated R820W variant affects NF-κB signaling and suppresses MYC transcriptional signatures

(A and B) Maximum relative expression values of NL *FLG* (A) and *S100A8* mRNA in the skin of children with AD in the MPAACH cohort by rs11652075 genotype. CC: n = 208; CT: n = 227; TT: n = 69. Median and interquartile range are shown. The simple linear regression b coefficients and p values of the indicated groupings on log-transformed expression values are shown.

(C) Relative luciferase activity in HEK293T cells transfected with the indicated plasmid and stimulated with PMA and ionomycin for 24 h. Values normalized to cells transfected with WT plasmid. Means and SDs are shown. Each symbol represents matched values from an independent replicate (n = 5). Each replicate was normalized to WT; one-sample t tests were used to test whether the mean of each experimental group was different from 1 (represented by the dotted line).

(D) Schematic of the RNA-seq experiment between WT and isogenic R820W HaCaT keratinocytes treated with 24 h mepazine or DMSO vehicle ($n = 3$).
(E) GSEA plots of the Hallmark MYC Target V1 and V2 pathways in R820W + V vs. WT + V cells.
(F) IPA Upstream Regulators analysis.
(G) IPA Molecular and Cellular Functions analysis.
(H) Graphical summary of the IPA Network Analysis highlighting the central location of the MYC node.
See also Figure S2.

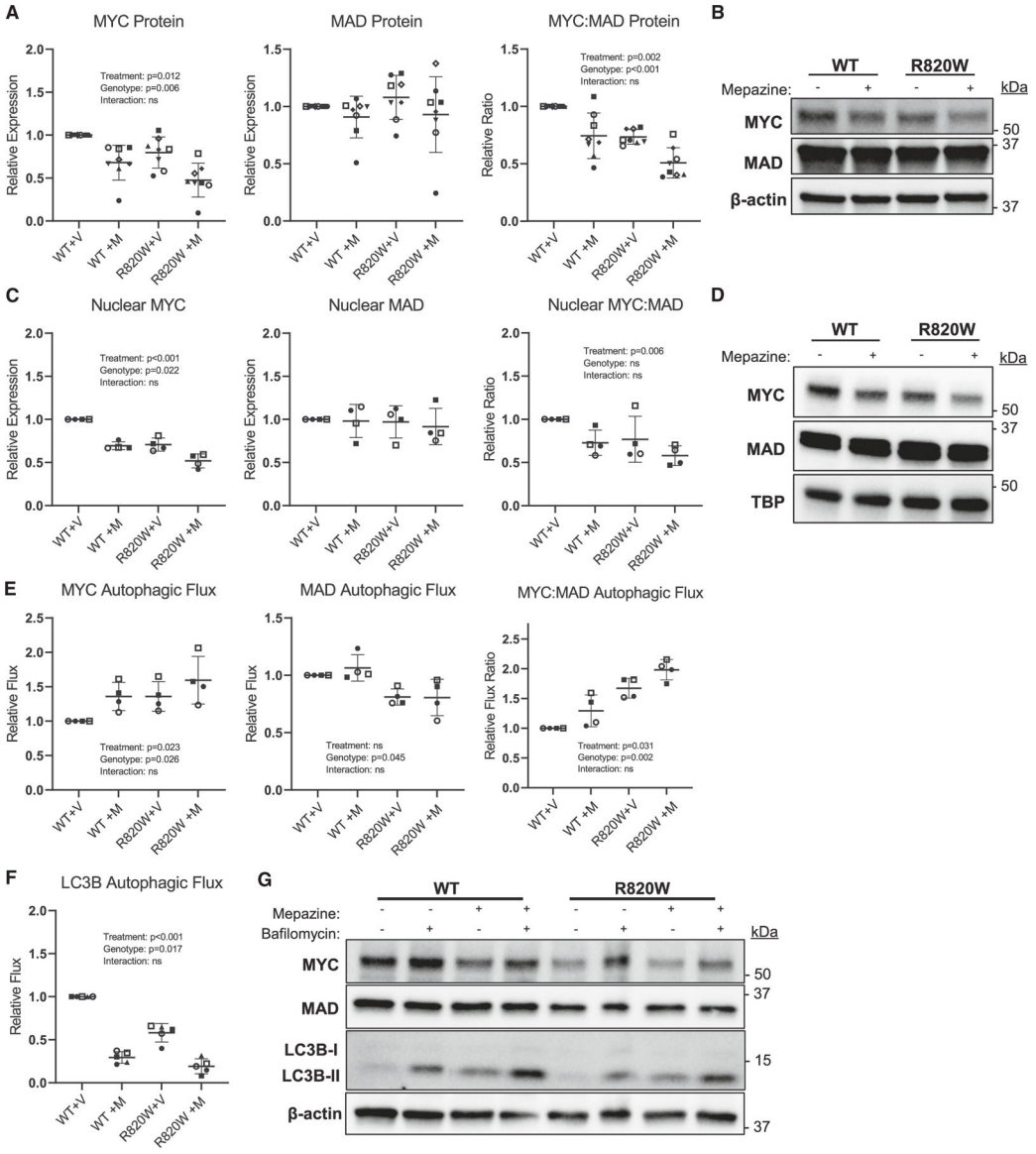

Figure 2. MYC levels are reduced, but MYC autophagy is elevated in R820W and mepazine-treated keratinocytes

(A and B) Quantification (A) and representative blot (B) of relative expression of total cellular MYC, MAD, and their ratio under each treatment condition. Each symbol represents matched values from an independent replicate ($n = 8$).

(C and D) Quantification (C) and representative blot (D) of relative expression of nuclear MYC, MAD, and their ratio under each treatment condition. Each symbol represents matched values from an independent replicate ($n = 4$).

(E and F) Quantification of relative autophagic flux of cellular MYC, MAD, and their ratio (E, $n = 4$) and LC3B (F, $n = 5$) under each treatment condition ±3 h bafilomycin. Each symbol represents matched values from an independent replicate.

(G) Representative blot quantified in (E) and (F). Means and SDs are shown in all graphs. Means separated by paired two-way ANOVAs and Tukey post hoc tests.

See also Figures S3 and S4.

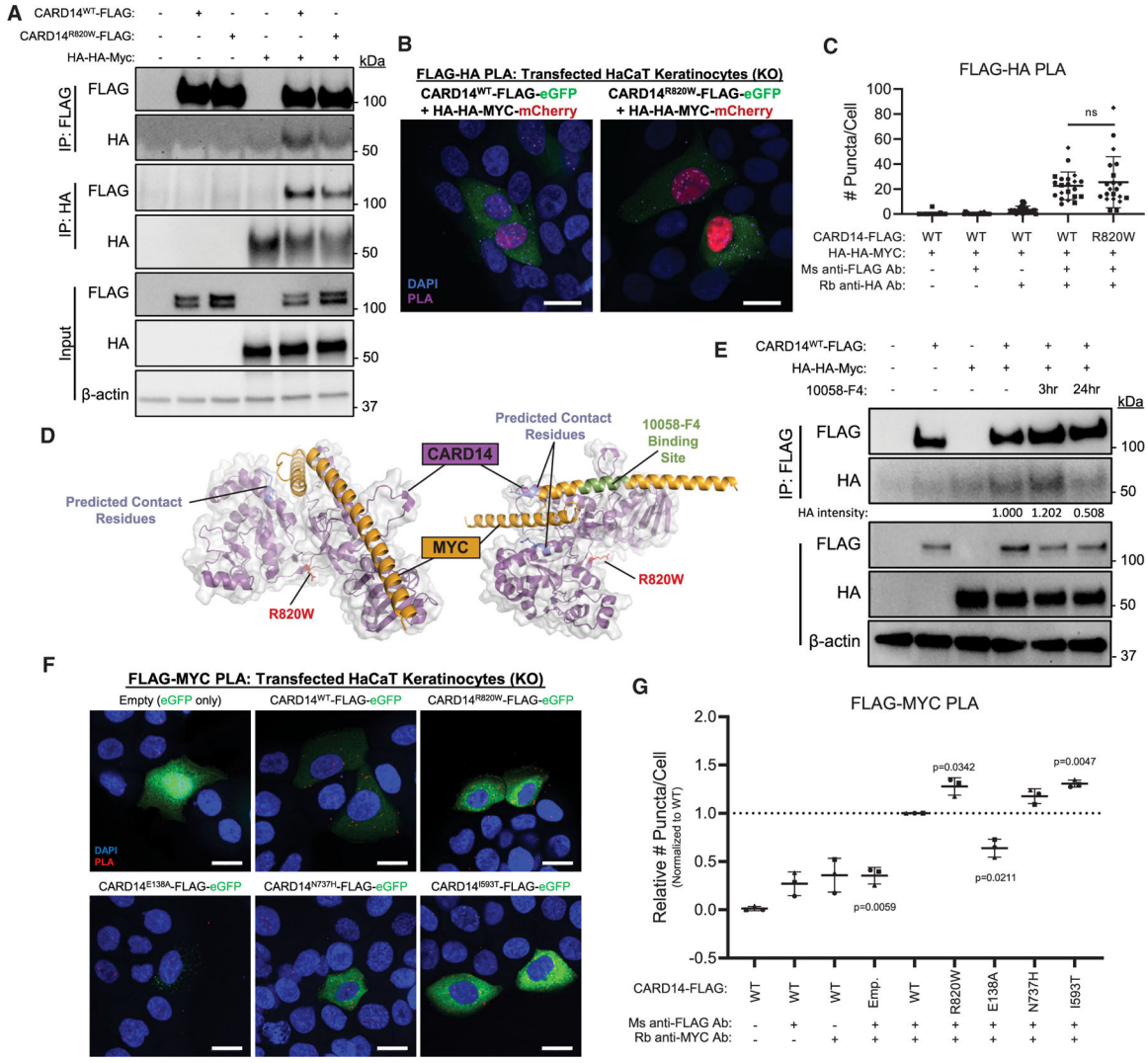

Figure 3. Direct CARD14 and MYC binding in keratinocytes is dependent on CARD14 activation status and the presence of disease-associated CARD14 variants

(A) Representative blot of IPs between tagged CARD14 and MYC expressed in KO HaCaT keratinocytes ($n = 3$).

(B and C) Representative images (B) and quantification (C) of PLAs between tagged MYC and CARD14 expressed in KO keratinocytes. Each point represents puncta counts from one cell. Matching symbols represent data points from cells within the same replicate (≥5 co-transfected cells per condition per replicate, $n = 3$ replicates). Means separated by a paired two-tailed t test of average puncta counts per replicate. Means and SDs are shown. Scale bars, 50 μM.

(D) *In silico* model of the predicted interaction between the membrane-associated guanylate kinase domain of CARD14 and the basic-helix-loop-helix domain of MYC. The 10058-F4 binding site on MYC is indicated.

(E) Representative blot of IPs of KO HaCaT keratinocytes transfected with CARD14 and MYC ±10058-F4 treatment 24 before harvest ($n = 3$). Relative intensities of MYC bands are shown.

(F and G) Representative images (F) and quantification (G) of PLAs between endogenous MYC and tagged CARD14 constructs transfected into KO keratinocytes with 3 h bafilomycin (to prevent MYC degradation) and 1 h PMA and ionomycin (to activate CARD14) treatment prior to fixation. Each symbol represents matched values from an independent replicate (≥6 cells per condition per replicate; $n = 3$ replicates). Each replicate was normalized to WT; one-sample t tests were used to test whether the mean of each experimental group was different from 1 (represented by the dotted line). Means and SDs are shown. Scale bars, 20 μM.

See also Figure S5.

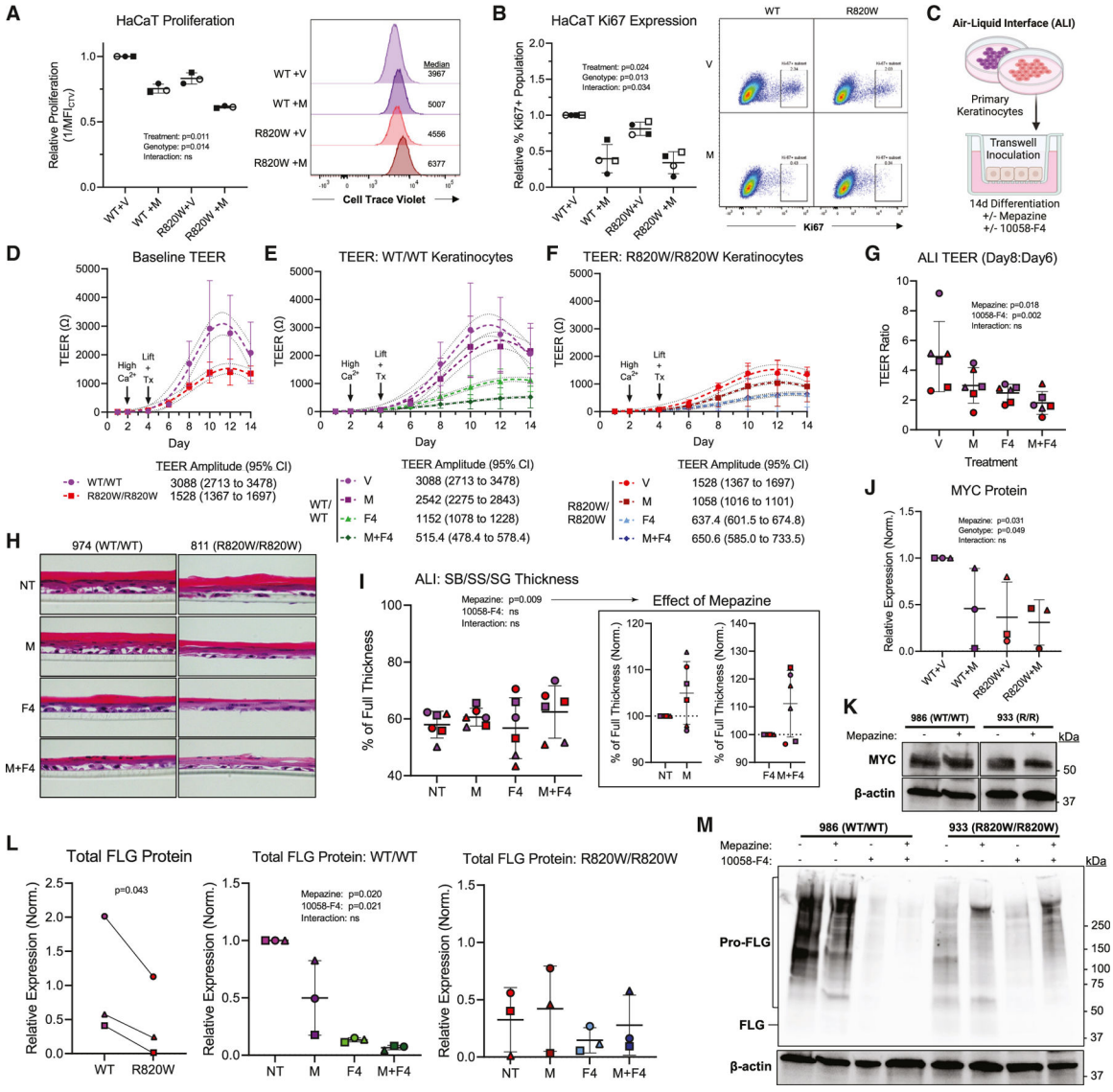

Figure 4. CARD14-MYC signaling regulates keratinocyte proliferation and epidermal barrier function

(A and B) Quantification and representative flow plots of the proliferation of WT vs. R820W HaCaT cells (±mepazine) as determined by dye dilution (A, $n = 3$) and % Ki67 expression (B, $n = 4$). Each symbol represents matching values from independent replicates. Means and SDs are shown.

(C) The ALI model.

(D–F) Longitudinal TEERs of homozygous WT or R820W ALIs at baseline (D), and with mepazine and/or 10058-F4 treatment (E and F). Maximum TEERs and CIs are shown.

(G) Ratio of day 8:day 6 TEERs.

(H) Representative ALI H&Es.

(I) Quantification of the combined thicknesses of basal, spinous, and granular layers as a percentage of full thickness; inset normalizes to untreated to highlight the effect of mepazine.

(J and K) Quantification (J) and representative blot (K) of MYC protein expression in ALIs under the indicated condition.

(L and M) Quantification (L) and representative blot (M) of FLG protein expression in ALIs under the indicated condition. For all ALI experiments, $n = 3$ keratinocyte strains per genotype. Each strain and genotype is represented by a different symbol and color (purple = WT, red = R820W). Means and SDs are shown.

For inset in (I) and WT vs. R820W FLG in (L), means were separated by a two-tailed paired t test. In (L), the ALIs of each genotype that were grown concurrently were used to pair the samples for statistical purposes. For all other quantifications, means were separated by paired two-way ANOVAs and Tukey post hoc tests. F4, 10058-F4; SB, stratum basale; SG, stratum granulosum; SS, stratum spinosum. See also Figures S6 and S7.

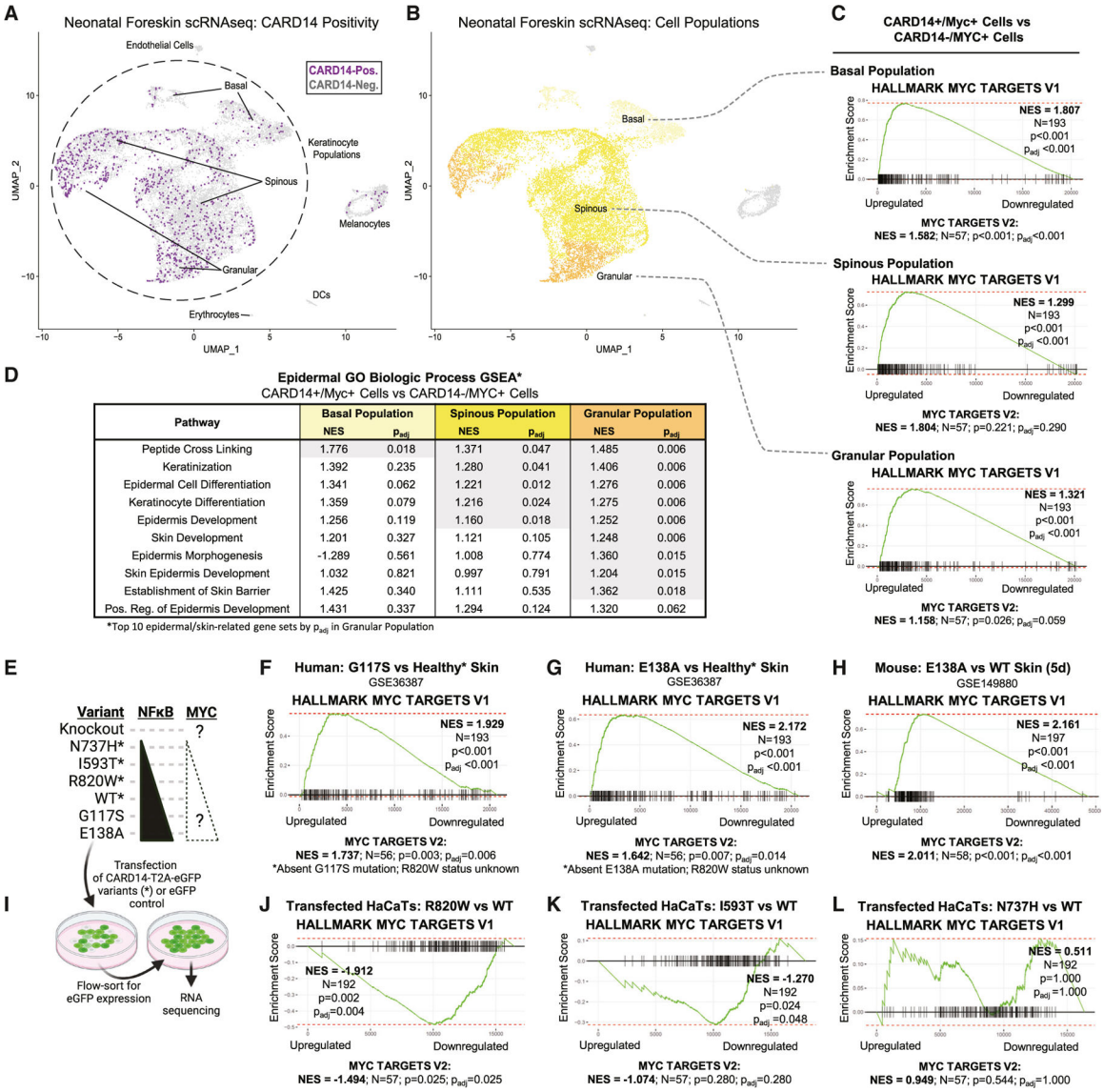

Pathway	Basal Population		Spinous Population		Granular Population	
	NES	p_{adj}	NES	p_{adj}	NES	p_{adj}
Peptide Cross Linking	1.776	0.018	1.371	0.047	1.485	0.006
Keratinization	1.392	0.235	1.280	0.041	1.406	0.006
Epidermal Cell Differentiation	1.341	0.062	1.221	0.012	1.276	0.006
Keratinocyte Differentiation	1.359	0.079	1.216	0.024	1.275	0.006
Epidermis Development	1.256	0.119	1.160	0.018	1.252	0.006
Skin Development	1.201	0.327	1.121	0.105	1.248	0.006
Epidermis Morphogenesis	-1.289	0.561	1.008	0.774	1.360	0.015
Skin Epidermis Development	1.032	0.821	0.997	0.791	1.204	0.015
Establishment of Skin Barrier	1.425	0.340	1.111	0.535	1.362	0.018
Pos. Reg. of Epidermis Development	1.431	0.337	1.294	0.124	1.320	0.062

Figure 5. CARD14-MYC signaling promotes epidermal differentiation in vivo, and MYC signaling is altered downstream of pathogenic CARD14 variants

(A and B) Uniform manifold approximation and projections of scRNA-seq data showing CARD14-positive vs. CARD14-negative cells (A) and epidermal layer cell populations (B) in foreskin epidermal keratinocytes from five donors (GEO: GSE147482; 16,981 total cells). DC, dendritic cell.

(C) GSEA results of the Hallmark MYC Target V1 and V2 pathways in $CARD14^{+}/MYC^{+}$ vs. $CARD14^{-}/MYC^{+}$ cells within each epidermal layer cell population.

(D) GSEA normalized enrichment score (NES) and p_{adj} values of GO terms related to epidermal differentiation in $CARD14^{+}/MYC^{+}$ vs. $CARD14^{-}/MYC^{+}$ cells within each epidermal layer cell population.

(E) Schematic of NF-κB and MYC activity in pathogenic CARD14 variants.

(F–H) GSEA results of the Hallmark MYC pathways in the skin of individuals with PsV^{+} *CARD14*^{G117S} vs. healthy (F), the skin of an individual with GPP^{+} *CARD14*^{E138A}

vs. healthy (G), and the skin of mice 5 days after tamoxifen induction of *Card14*^{E138A} vs. WT (H).

(I) Schematic of the RNA-seq experiment between fluorescence-activated cell sorting-sorted KO HaCaT keratinocytes transfected with the variants indicated in (E).

(J–L) GSEA results of the Hallmark MYC pathways in the KO HaCaT cells transfected with *CARD14*^{R820W} (J), *CARD14*^{I593T} (K), or *CARD14*^{N737H} (L) vs. *CARD14*^{WT} ($n = 2$).

See also Figure S8.

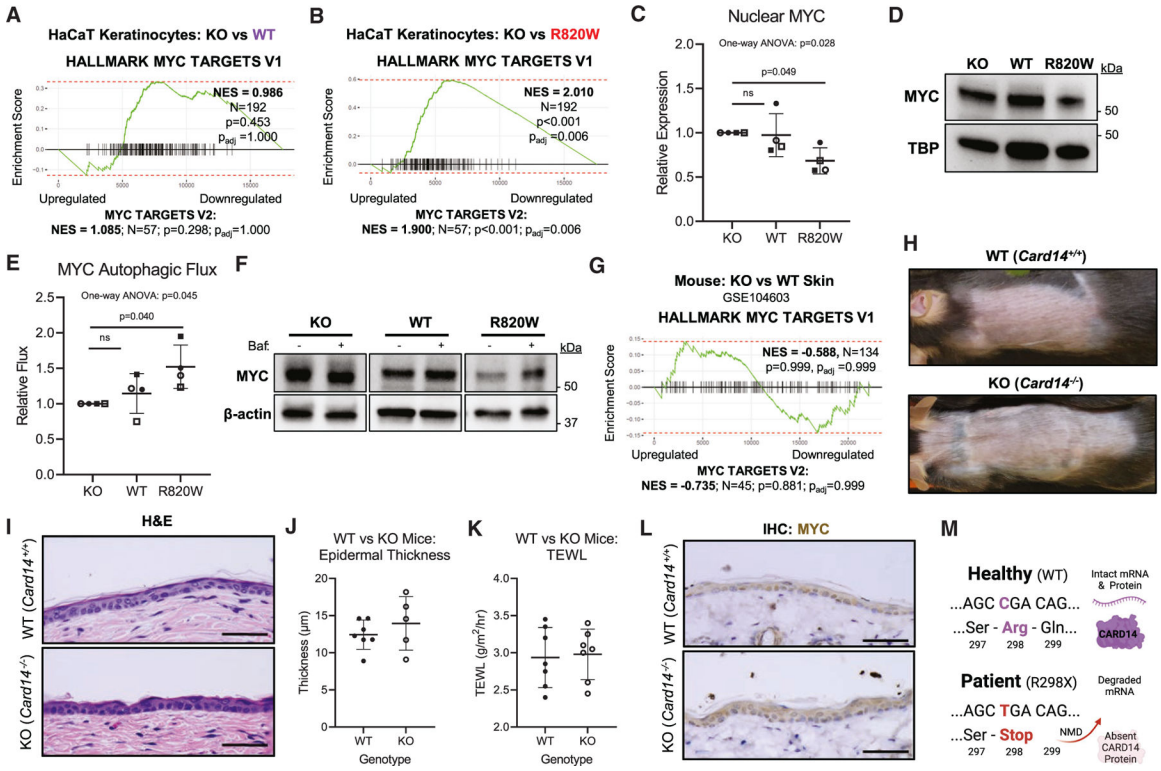

Figure 6. MYC signaling is preserved in the absence of CARD14 protein, and AD is absent in a rare case of human CARD14 deficiency

(A and B) GSEA results of the Hallmark MYC Target V1 and V2 pathways in KO vs. WT (A) or R820W (B) HaCaT keratinocytes.

(C and D) Quantification (C) and representative blot (D) of baseline nuclear MYC in each cell type.

(E and F) Quantification (E) and representative blot (F) of baseline MYC autophagy in each cell type.

Each symbol in (C) and (E) represents matched values from an independent replicate ($n = 4$). Means separated by paired one-way ANOVAs and Tukey post hoc tests. Means and SDs are shown.

(G) GSEA results of the Hallmark MYC pathways in *Card14*-deficient vs. WT mouse skin.

(H and I) Representative images of the gross (H) and histologic (I) phenotypes of the skin of *Card14*-deficient vs. WT mice.

(J) Quantification of epidermal thickness in *Card14*-deficient ($n = 5$) vs. WT mice ($n = 7$).

(K) Quantification of TEWL in *Card14*-deficient ($n = 7$) vs. WT mice ($n = 7$).

For (J) and (K), means separated with two-tailed t tests; means and SDs are shown.

(L) Representative images of MYC expression in the skin of *Card14*-deficient vs. WT mice.

(M) Schematic of the human $CARD14^{R298X}$ truncation mutation.

Baf., bafilomycin. Scale bars, 50 μM.

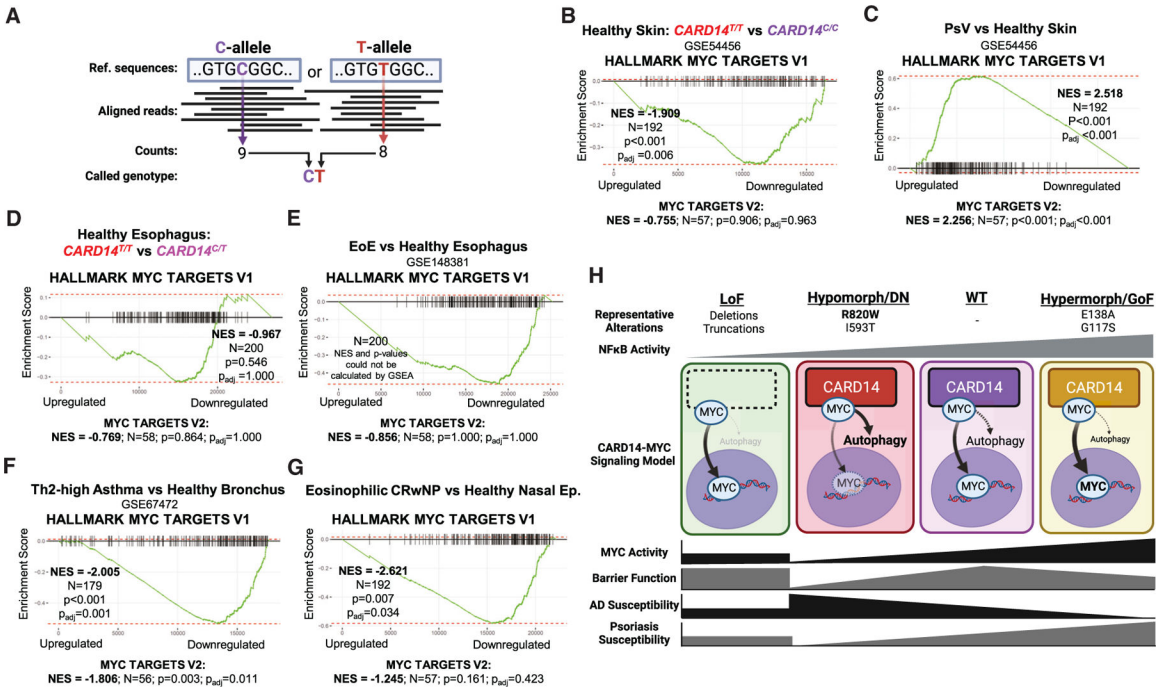

Figure 7. Altered CARD14-MYC signaling may contribute to barrier homeostasis and allergic disease in other epithelial tissues

(A) Schematic of calling rs11652075 genotypes using RNA-seq reads.

(B–G) GSEA results of the Hallmark MYC pathways in between rs11652075 genotypes within healthy tissues (B and D) or between diseased vs. healthy tissues (C and E–G).

(H) Working model representing how representative CARD14 variants impact MYC signaling to alter barrier function and predispose to inflammatory skin disease.

See also Figure S9.

KEY RESOURCES TABLE

REAGENT or RESOURCE	SOURCE	IDENTIFIER
Antibodies		
FLAG tag M2 (mouse) (IP (1:50), WB (1:1000), IF (1ug/mL), PLA (1ug/mL))	Sigma Aldrich, St. Louis, MO	Cat# F1804; RRID: AB_262044
Beta-actin (mouse) (WB (1:2000))	Abcam, Cambridge, United Kingdom	Cat# ab8226; RRID: AB_306371
MYC (rabbit) (WB (1:1000), IF (HaCaT: 0.25μg/mL; ESS: 1:50), PLA (0.25μg/mL))	Cell Signaling Technologies, Danvers, MA	Cat# 9402; RRID: AB_2141827
MYC (rabbit)- for mouse IHC only (IHC (1:200))	Abcam, Cambridge, United Kingdom	Cat# Ab32072; RRID: AB_731658
MAD (rabbit) (WB (1:1000))	ThermoFisher Scientific, Waltham, MA	Cat# PA5–100285; RRID: AB_2849799
p-ERK (rabbit) (WB (1:1000))	Cell Signaling Technologies, Danvers, MA	Cat# 4370; RRID: AB_2315112
ERK (rabbit) (WB (1:1000))	Cell Signaling Technologies, Danvers, MA	Cat# 4695; RRID: AB_390779
HA-tag (rabbit) (IP (1:50), WB (1:1000), PLA (0.0132μg/mL))	Cell Signaling Technologies, Danvers, MA	Cat# 3724; RRID: AB_1549585
TBP (rabbit) (WB (1:2000))	Cell Signaling Technologies, Danvers, MA	Cat# 44059; RRID: AB_2799258
LC3A/B (rabbit) (WB (1:1000))	Cell Signaling Technologies, Danvers, MA	Cat# 4108; RRID: AB_2137703
6x-His-tag (mouse) (IP (1:50), WB (1:1000))	ThermoFisher Scientific, Waltham, MA	Cat# MA1–21315; RRID: AB_557403
Ki67-BUV737 (mouse) (Flow (1:25))	ThermoFisher Scientific, Waltham, MA	Cat# 367–5699-42; RRID: AB_2896018
Filaggrin (mouse) (WB (1:200))	Santa Cruz Biotechnology, Dallas, TX	Cat# sc-66192; RRID: AB_1122916
CARD14 (mouse) (PLA (20μg/mL))	Abcam, Cambridge, United Kingdom	Cat# ab168096
anti-Rabbit-HRP (goat) (WB (1:10,000))	Abcam, Cambridge, United Kingdom	Cat# ab6721; RRID: AB_955447
anti-Mouse-HRP (goat) (WB (1:10,000))	Abcam, Cambridge, United Kingdom	Cat# ab205719; RRID: AB_2755049
anti-Rabbit-AlexaFluor594 (IF (1ug/mL))	Jackson ImmunoResearch, West Grove, PA	Cat# 111–585-003; RRID: AB_2338059
anti-Rabbit-biotinylated (IHC (1:200))	Vector Laboratories, Newark, CA	Cat# BA-1000; RRID: AB_2313606
VeriBlot (WB (1:1000))	Abcam, Cambridge, United Kingdom	Cat# ab131366; RRID: AB_2892718
Chemicals, peptides, and recombinant proteins		
DMEM, low glucose, GlutaMAX Supplement, pyruvate	ThermoFisher Scientific, Waltham, MA	10–567-022
Dulbecco's Modified Eagles Medium (DMEM)/Nutrient Mixture F-12 Ham	Sigma Aldrich, St. Louis, MO	D2906
Medium 154	ThermoFisher Scientific, Waltham, MA	M154500
DME powder	ThermoFisher Scientific, Waltham, MA	31600
Human Keratinocyte Growth Supplement (HKGS)	ThermoFisher Scientific, Waltham, MA	S0015
Fetal Bovine Serum	ThermoFisher Scientific, Waltham, MA	MT35015CV
Antibiotic-Antimycotic Solution (100X)	Caisson Labs, Smithfield, UT	ABL02

REAGENT or RESOURCE	SOURCE	IDENTIFIER
Bovine Pituitary Extract	Cell Applications, San Diego, CA	1078-NZ
Insulin-Transferrin-Selenium (ITS) Supplement	Sigma Aldrich, St. Louis, MO	I3146
Keratinocyte Growth Factor (KGF)	Peprotech, Rocky Hill, NJ	100–19
Basic Fibroblast Growth Factor	Peprotech, Rocky Hill, NJ	100–18B
Epidermal Growth Factor (EGF)	Peprotech, Rocky Hill, NJ	AF100–15
L-Ascorbic Acid 2-Phosphate	Sigma Aldrich, St. Louis, MO	A8960–5G
Hydrocortisone	Sigma Aldrich, St. Louis, MO	H4001
Insulin	Sigma Aldrich, St. Louis, MO	I2643
Strontium Chloride	Sigma Aldrich, St. Louis, MO	255521
Triiodothyronine	Sigma Aldrich, St. Louis, MO	T5516
Linoleic Acid	Sigma Aldrich, St. Louis, MO	L9530
Lipofectamine 3000 Transfection Reagent	ThermoFisher Scientific, Waltham, MA	L3000015
Mepazine Hydrochloride (MALT1 Inhibitor II) (10μM)	Sigma Aldrich, St. Louis, MO	5.01E+09
Phorbol Myristate Acetate (PMA) (80 ng/mL)	Sigma Aldrich, St. Louis, MO	P8139
Ionomycin (1 mM)	Sigma Aldrich, St. Louis, MO	407952
10058-F4 (cMYC-MAX dimerization inhibitor) (12.5uM)	Abcam, Cambridge, United Kingdom	ab145065
Actinomycin D (10μg/mL)	Cell Signaling Technologies, Danvers, MA	15021
Bafilomycin A1 Ready Made Solution (200nM)	Sigma Aldrich, St. Louis, MO	SML-1661
Cycloheximide (50μg/mL)	Sigma Aldrich, St. Louis, MO	C4859
MG132 (10μM)	Sigma Aldrich, St. Louis, MO	M8699
Mitomycin C (20μM)	Sigma Aldrich, St. Louis, MO	M4287
Acridine Orange 10-Nonyl Bromide (NAO) (100nM)	ThermoFisher Scientific, Waltham, MA	A1372
Tetramethylrhodamine ethyl ester (TMRE) (50nM)	Abcam, Cambridge, United Kingdom	ab113852
DAPI	ThermoFisher Scientific, Waltham, MA	D1306
Cell Trace Violet	ThermoFisher Scientific, Waltham, MA	C34571
LIVE/DEAD Fixable Near-IR Dead Cell Stain Kit	ThermoFisher Scientific, Waltham, MA	L10119
SuperScript IV VILO Master Mix	ThermoFisher Scientific, Waltham, MA	11756500
Taqman Fast Advanced Master Mix	ThermoFisher Scientific, Waltham, MA	4444965
Halt Protease Inhibitor Cocktail	ThermoFisher Scientific, Waltham, MA	78428
Halt Phosphatase Inhibitor Cocktail	ThermoFisher Scientific, Waltham, MA	78430
Protein G Dynabeads	ThermoFisher Scientific, Waltham, MA	10–004-D
EveryBlot Blocking Buffer	Bio-Rad, Hercules, CA	12010020
10x Tris/Glycine/SDS Buffer	Bio-Rad, Hercules, CA	1610772
Precision Plus Protein Dual Color Standards	Bio-Rad, Hercules, CA	1610374
Immobilon Forte Western HRP substrate	Millipore Sigma, Burlington, MA	WBLUF0100
Restore PLUS Western Blot Stripping Buffer	ThermoFisher Scientific, Waltham, MA	46430
Normal Donkey Seurm	Sigma Aldrich, St. Louis, MO	D9663
TrueVIEW Autofluorescence Quenching Kit	Vector Laboratories, Newark, CA	SP-8400–15
VECTASTAIN ABC-HRP Kit, Peroxidase	Vector Laboratories, Newark, CA	PK-4000
DAB Substrate Kit, Peroxidase (HRP), with Nickel	Vector Laboratories, Newark, CA	SK-4100
ProLong Diamond Antifade Mountant	ThermoFisher Scientific, Waltham, MA	P36965
eBioscience IC Fixation and Permeabilization Buffer Set	ThermoFisher Scientific, Waltham, MA	88–8824-00

REAGENT or RESOURCE	SOURCE	IDENTIFIER
Critical commercial assays		
MYC Taqman probe	ThermoFisher Scientific, Waltham, MA	Hs00153408_m1
MXD1 Taqman probe	ThermoFisher Scientific, Waltham, MA	Hs00965581_m1
FLG Taqman probe	ThermoFisher Scientific, Waltham, MA	Hs00856927_g1
S100A8 Taqman probe	ThermoFisher Scientific, Waltham, MA	Hs00374264_g1
GAPDH Taqman probe	ThermoFisher Scientific, Waltham, MA	Hs02758991_g1
18S Taqman probe	ThermoFisher Scientific, Waltham, MA	Hs03003631_g1
Seahorse XF DMEM assay medium pack, pH 7.4	Agilent, Santa Clara, CA	103680–100
Seahorse XFe96 FluxPak	Agilent, Santa Clara, CA	102601–100
Seahorse XF Real-Time ATP Rate Assay Kit	Agilent, Santa Clara, CA	103592–100
Dual-Luciferase Reporter Assay System (for NF-κB activity)	Promega, Madison, WI	E1910
Pierce BCA Protein Assay	ThermoFisher Scientific, Waltham, MA	23227
NaveniFlex MR	Navinci Diagnostics, Uppsala, Sweden	NF.MR.100
Infinium Multi-Ethnic Global-8 v1.0 Kit	Illumina, San Diego, CA	WG-316–1003
Deposited data		
RNA-sequencing; Human HaCaT keratinocytes (WT, R820W, KO) +/− DMSO and/or Mepazine	This study	GEO: GSE263420
RNA-sequencing; Human KO HaCaT keratinocytes transfected with CARD14 variants	This study	GEO: GSE263428
Single-cell sequencing; Human Neonatal Foreskin Epidermis	(Wang et al.)[29]	GEO: GSE147482
RNA-sequencing; Human full-thickness skin PsV vs. GPP vs. Healthy	(Jordan et al.)[30]	GEO: GSE36387
RNA-sequencing; Mouse whole ear skin, Inducible Card14^{E138A}, Card14$^{+/+}$	(Manils et al.)[31]	GEO: GSE149880
RNA-sequencing; Mouse whole ear skin, Card14$^{-/-}$, Card14$^{+/+}$	(Tanaka et al.)[35]	GEO: GSE104603
RNA-sequencing; Human full-thickness skin; psoriatic vs. healthy	(Li et al.)[40]	GEO: GSE54456
RNA-sequencing; Human esophagus; eosinophilic esophagitis vs. healthy	(Greuter et al.)[44]	GEO: GSE148381
RNA-sequencing; Human bronchus; Th2-high asthma vs. healthy	(Christenson et al.)[46]	GEO: GSE67472
RNA-sequencing; Human nasal epithelium; eosinophilic CRwNP vs. healthy	(Wang et al.)[47]	GEO: GSE72713
RNA-sequencing; Human keratinocyte transfected with CARD14 variants	(Jordan et al.)[18]	GEO: GSE36381
RNA-sequencing; Human skin; psoriatic and healthy skin with secukinumab	(Liu et al.)[42]	GEO: GSE171012
Experimental models: Cell lines		
HaCaT Human Keratinocytes	Cell Line Services	N/A
Experimental models: Organisms/strains		
Human Primary Keratinocytes	This study (see Table S4)	N/A
Mice: Wild-type C57BL/6J	Jackson Labs	000664
Mice: CARD14$^{-/-}$	(Tanaka et al.)[35]	N/A

REAGENT or RESOURCE	SOURCE	IDENTIFIER
Oligonucleotides		
Oligo (Cloning): FLAG-T2A sequence (Fwd.) (CGCGTGATTACAAGGATGACGACGATAAGGGCAGTG GAGAGGGCAGAGGAAGTCTGCTAACATGCGGTGACGT CGAGGAGAATCCTGGCCCACCGC)	Integrated DNA Technologies, Coralville, IA	N/A
Oligo (Cloning): FLAG-T2A sequence (Rev.) (GGCCGCGGTGGGCCAGGATTCTCCTCGACGTCACCG CATGTTAGCAGACTTCCTCTGCCCTCTCCACTGCCCTT ATCGTCGTCATCCTTGTAATCA)	Integrated DNA Technologies, Coralville, IA	N/A
Oligo (Site-Directed Mutagenesis): CARD14 R820W– > WT conversion (Fwd.) (TACCCTGGTGCGGCCCCATCG)	Integrated DNA Technologies, Coralville, IA	N/A
Oligo (Site-Directed Mutagenesis): CARD14 R820W– > WT conversion (Rev.) (TAGGGCACCAGGGTGAGG)	Integrated DNA Technologies, Coralville, IA	N/A
Oligo (Site-Directed Mutagenesis): CARD14 WT– > E138A conversion (Fwd.) (CTGCAGGAGGCGCTGAACCAGGAAAAGG)	Integrated DNA Technologies, Coralville, IA	N/A
Oligo (Site-Directed Mutagenesis): CARD14 WT– > E138A conversion (Rev.) (GCTGCCGATGGCCCCAGC)	Integrated DNA Technologies, Coralville, IA	N/A
Oligo (Site-Directed Mutagenesis): CARD14 WT– > I593T conversion (Fwd.) (CTCACGGGCACCTTCATCCACC)	Integrated DNA Technologies, Coralville, IA	N/A
Oligo (Site-Directed Mutagenesis): CARD14 WT– > I593T conversion (Rev.) (GTTCCCGCCGATGACGCT)	Integrated DNA Technologies, Coralville, IA	N/A
Oligo (Site-Directed Mutagenesis): CARD14 WT– > N737H conversion (Fwd.) (CACCATCCCCCACTACTCCAGGG)	Integrated DNA Technologies, Coralville, IA	N/A
Oligo (Site-Directed Mutagenesis): CARD14 WT– > N737H conversion (Rev.) (CCGTGCGCGGCAGTATCC)	Integrated DNA Technologies, Coralville, IA	N/A
Oligo (Site-Directed Mutagenesis): T2A removal from CARD14 plasmids (Fwd.) (CCGCGGCCGCTCGAGATG)	Integrated DNA Technologies, Coralville, IA	N/A
Oligo (Site-Directed Mutagenesis): T2A removal from CARD14 plasmids (Rev.) (TCCACTGCCCTTATCGTCGTCATC)	Integrated DNA Technologies, Coralville, IA	N/A
Oligo (Site-Directed Mutagenesis): 6xHis addition to CARD10 (Fwd.) (CACCACCATCACTAAACGGCCGGCCGCGGTCAT)	Integrated DNA Technologies, Coralville, IA	N/A
Oligo (Site-Directed Mutagenesis): 6xHis addition to CARD10 (Rev.) (ATGGTGACCACCACCACGCGTGGCCTCACTGCTGC)	Integrated DNA Technologies, Coralville, IA	N/A
pcDNA3-eGFP plasmid	Doug Golenbock Lab (unpublished plasmid)	Doug Golenbock Lab Addgene 13031
CARD14 (NM_024110) Human Tagged ORF Clone plasmid	Origene Technologies, Rockville, MD	RC217455
pcDNA3-HA-HA-human-cMYC plasmid	(Vo et al.)[53]	Martine Roussel Lab Addgene 74164
pCas9-mCherry plasmid	(Schmid-Burgk et al.)[54]	Veit Hornung Lab Addgene 80975
CARD10 (NM_014550) Human Tagged ORF Clone plasmid	Origene Technologies, Rockville, MD	RC217652
pNL3.2.NF-kB-RE[NlucP/NF-kB-RE/Hygro] Vector plasmid	Promega, Madison, WI	N1111
pGL4.50[luc2/CMV/Hygro] Vector plasmid	Promega, Madison, WI	E1310
CARD14WT-FLAG-T2A-eGFP plasmid	This study	N/A
CARD14WT-FLAG-eGFP plasmid	This study	N/A
CARD14R820W-FLAG-T2A-eGFP plasmid	This study	N/A
CARD14R820W-FLAG-eGFP plasmid	This study	N/A
CARD14E138A-FLAG-T2A-eGFP plasmid	This study	N/A

REAGENT or RESOURCE	SOURCE	IDENTIFIER
CARD14E138A-FLAG-eGFP plasmid	This study	N/A
CARD14I593T-FLAG-T2A-eGFP plasmid	This study	N/A
CARD14I593T-FLAG-eGFP plasmid	This study	N/A
CARD14N737H-FLAG-T2A-eGFP plasmid	This study	N/A
CARD14N737H-FLAG-eGFP plasmid	This study	N/A
HA-HA-MYC-mCherry plasmid	This study	N/A
Software and algorithms		
LightCycler 96 Software	Roche, Indianapolis, IN	N/A
Applied Biosystems Analysis Software	ThermoFisher Scientific, Waltham, MA	N/A
ThermoFisher Connect Software	ThermoFisher Scientific, Waltham, MA	N/A
Image Lab 6.1	Bio-Rad, Hercules, CA	N/A
Imaris	Oxford Instruments, Abingdon, UK	N/A
NIS Elements AR	Nikon, Melville, NY	N/A
Agilent Seahorse Analytics	Agilent, Santa Clara, CA	N/A
Zen 3.3 Blue	Zeiss, Oberkochen, Germany	N/A
FlowJo (v10.8.1)	BD Biosciences, Franklin Lakes, NJ	N/A
GraphPad Prism 9	GraphPad Software, Boston, MA	N/A
Ingenuity Pathway Analysis	Qiagen, Hilden, Germany	N/A
Clustal O (1.2.4)	N/A	N/A
iLINCS	N/A	N/A
R and R Studio	N/A	N/A
Python	N/A	N/A
Other		
BD Vacutainer Plastic Blood Collection Tubes with K2 EDTA: Hemogard Closure	ThermoFisher Scientific, Waltham, MA	23–021-015
BD Vacutainer Glass Mononuclear Cell Preparation Tubes	ThermoFisher Scientific, Waltham, MA	14–949-51D
12mm Transwell (0.4uM pore)	Corning, Corning, NY	3460
Polyvinyl Acetal Sponges	Carwild, New London, CT	N/A
Dneasy Blood & Tissue Kit	Qiagen, Hilden, Germany	69506
OGR-675 Kit	DNA Genotek, Ottawa, Ontario, Canada	OGR-675
prepIT-2LP Kit	DNA Genotek, Ottawa, Ontario, Canada	PT-L2P-45
SmartSolve Dissolving Tape	Smartsolve, Bowling Green, OH	IT112021S
ReliaPrep RNA Miniprep System	Promega, Madison, WI	Z6012
Q5 Site Directed Mutagenesis Kit	New England Biolabs, Ipswich, MA	E0554S
8-well Chamber Slide with Removable Silicone Wells	Ibidi, Fitchburg, WI	80841
4–15% Mini-PROTEAN TGX Precast Protein Gels (10 wells)	Bio-Rad, Hercules, CA	4561084
4–15% Mini-PROTEAN TGX Precast Protein Gels (15 wells)	Bio-Rad, Hercules, CA	4561086
Immun-Blot PVDF Membrane	Bio-Rad, Hercules, CA	1620174